Ecological Processes

RESEARCH

Open Access

An 1800-year record of *Austrocedrus chilensis* growth reveals an unprecedented recent decline in the Patagonian forest–steppe ecotone

Daiana Wouters[1*], Duncan A. Christie[2,3,4], Carlos LeQuesne[2], Eugenia Marcotti[5], Leticia María Vega[1,6], Ignacio Mundo[1,7], Tania Gipoulou-Zúñiga[2], Moisés Rojas-Badilla[2], Ana Srur[1], Mariano Masiokas[1] and Ricardo Villalba[1,4*]

Abstract

Background Recent decades brought persistent warming and declining precipitation to the North Patagonian Andes, raising concerns about the capacity of temperate mountain forests to withstand climate stress at the semi-arid forest–steppe ecotone. We assess whether current growth declines in *Austrocedrus chilensis* are unprecedented in a late Holocene context and whether intensified drought has contributed to a weakening of the relationship between climate and tree growth.

Methods Increment cores from living trees were combined with subfossil cross-sections to develop cross-dated, millennial-length ring-width chronologies at three ecotonal sites in northern Patagonia. Site chronologies were standardized using multiple detrending approaches and integrated into a regional chronology. Recent growth trends were evaluated against long-term variability using chronology comparisons, climate–growth regression models, observed-minus-predicted residual analyses, and drought legacy approaches.

Results Sustained growing-season warming since mid-1970s, together with more frequent severe droughts after 1997, has induced persistent multi-year moisture deficits since 2009. Across all sites, recent decades show a pronounced, persistent decline in *A. chilensis* growth that remains evident after accounting for age-related trends and differences in intrinsic growth rates among trees. Millennial records were integrated into a composite regional chronology extending back to CE 178, with a robust common signal from CE 520 onward. For 1917–2022, warm-season temperature and annual precipitation explain 42% of tree-growth variance, increasing to 46% when long-memory hydroclimatic variables capturing multi-year moisture deficits are included. Consistently, model performance deteriorates from the mid-1990s onward, overestimating observed growth and suggesting a loss of stationarity in climate–growth relationships. Residual analyses further show that growth reductions intensify under higher antecedent composite stress and persist for several years after droughts, consistent with drought legacy effects.

Conclusions Our results reveal an unprecedented, persistent low-growth regime in ecotonal *A. chilensis* forests over the past two to three decades. This decline falls outside the range of natural variability observed

*Correspondence:
Daiana Wouters
dwouters@mendoza-conicet.gob.ar
Ricardo Villalba
ricardo@mendoza-conicet.gob.ar
Full list of author information is available at the end of the article

© The Author(s) 2026, modified publication 2026. **Open Access** This article is licensed under a Creative Commons Attribution 4.0 International License, which permits use, sharing, adaptation, distribution and reproduction in any medium or format, as long as you give appropriate credit to the original author(s) and the source, provide a link to the Creative Commons licence, and indicate if changes were made. The images or other third party material in this article are included in the article's Creative Commons licence, unless indicated otherwise in a credit line to the material. If material is not included in the article's Creative Commons licence and your intended use is not permitted by statutory regulation or exceeds the permitted use, you will need to obtain permission directly from the copyright holder. To view a copy of this licence, visit http://creativecommons.org/licenses/by/4.0/.

in the millennial-length records and is not captured by long-term climate–growth models, pointing to a weakening of the relationship between climate and radial growth under ongoing warming and recurrent drought. These findings identify antecedent stress and drought legacy effects as key drivers of current forest performance in Patagonian forest–steppe ecotone.

Keywords Dendrochronology, Forest-steppe ecotone, Drought legacy effect, Climate-growth relationship, Hydroclimatic variability

Background

A growing body of meteorological records and environmental proxies shows that the climate of the North Patagonian Andes has changed markedly in recent decades, both in long-term trends and in the frequency of extreme events (Villalba et al. 2012; Garreaud et al. 2013; Garreaud 2018; Morales et al. 2020; Wang et al. 2025). Instrumental observations provide clear evidence of persistent warming and widespread hydroclimatic decline, together with a poleward migration of the westerly wind belt (Goyal et al. 2021; O'Connor et al. 2021; Deng et al. 2022; Villamayor et al. 2021). These changes have been associated with reduced precipitation, diminished snow cover, glacier retreat, and lower river flows across the region (Boisier et al. 2018; Dussaillant et al. 2019; Masiokas et al. 2019). Sustained increases in temperature, combined with a regional decrease in precipitation, have also contributed to a greater frequency and persistence of extreme droughts since the mid-twentieth century (Rivera et al. 2017, 2021; Garreaud 2018). Tree-ring-based hydroclimatic reconstructions further show that this regional aridification is unprecedented over the last several centuries and has gradually intensified since the 1970s (Morales et al. 2020; Hadad et al. 2021). In this context of rapid climate change, rising temperatures and less frequent rainfall events are increasingly affecting forest dynamics in the northern Andean–Patagonian ecotone by disrupting the ecophysiological processes that regulate growth, reducing forest vigor, and triggering increasingly frequent episodes of decline and mortality (Villalba and Veblen 1998; Rodriguez-Catón et al. 2016; Vega et al. 2019).

Temperate forests in southwestern South America are distributed along steep environmental gradients shaped by the interaction of Pacific-dominated precipitation, marked climatic seasonality, and the high Andean topography (Veblen et al. 1996; Viale et al. 2019). Along these gradients, vegetation changes abruptly, particularly at the transition between the Andean forest and the Patagonian steppe east of the Andes. This forest–steppe ecotone, which is highly sensitive to changes in water availability (Kitzberger 2012), marks the eastern distributional limit of the iconic conifer *Austrocedrus chilensis* (ciprés de la cordillera).

Austrocedrus chilensis has a discontinuous distribution on both sides of the Andes. On the western slope in Chile, the species occurs mainly between 32° and 38° S, with few scattered stands farther south between 42° and 44° S (Donoso Zegers 1993). In Argentina, *A. chilensis* extends from 37° to 44° S, from west-central Neuquén to northwestern Chubut, with a more continuous distribution toward the southern part of its range (Veblen et al. 1995; Pastorino et al. 2015). This contrasting geographic pattern reflects the precipitation asymmetry imposed by the Andes and is associated with spatial differences in growth sensitivity to climate, demographic dynamics, and forest structure (Veblen et al. 1995).

In the eastern Andes of northern Patagonia, numerous studies have shown that radial growth of *A. chilensis* is negatively related to temperature and positively related to precipitation during the growing season, indicating that reduced rainfall combined with increased evaporative demand limits soil water availability and becomes a critical constraint on growth (Villalba et al. 1998; Marcotti et al. 2025; Vega et al. 2025). *Austrocedrus chilensis* is a conifer adapted to periods of water stress through xeromorphic leaves and early stomatal closure under dry conditions (Gyenge et al. 2005; Vega et al. 2025). Nevertheless, its vulnerability to severe drought has been widely documented across much of its distribution (Villalba and Veblen 1998; Le Quesne et al. 2006; Amoroso et al. 2012). In central Chile, the megadrought that began in 2010 has been associated with the lowest decadal growth of *A. chilensis* during the last millennium and with increased growth synchrony, reflecting the strong influence of prolonged warm-dry conditions on species performance (Garreaud et al. 2017; González de Andrés et al. 2025). This regional hydroclimatic shift has also been linked to widespread decline in woody species of central Chile (Miranda et al. 2023; González-Reyes et al. 2024).

Austrocedrus chilensis is particularly well suited for dendroclimatic studies because it frequently grows in xeric environments where water availability strongly limits radial growth (Schulman 1956). However, a common limitation for developing long tree-ring records from this species in Argentina is the difficulty of finding old stands without evidence of disturbance, particularly

fire (Kitzberger et al. 1997; Veblen et al. 1999). Since the 1980s, new collections have expanded the network of *A. chilensis* tree-ring chronologies in northern Patagonia (Villalba and Veblen 1997a; Villalba et al. 1998; Marcotti et al. 2025). These chronologies have supported studies of climate–growth relationships, drought-related mortality and decline at the forest–steppe boundary (Villalba and Veblen 1998; Mundo et al. 2010; Amoroso et al. 2012), and the influence of large-scale modes of climate variability on species growth (Villalba et al. 1998, 2012).

Despite extensive research across different portions of the forest–steppe ecotone, major knowledge gaps remain regarding how recent growth decline in *A. chilensis* should be interpreted in the context of long-term growth variability and ongoing warming and aridification. Although existing chronologies show strong growth responses to water availability, several studies indicate that the spatial variability of these responses remains incompletely explained and that temporal changes in climate–growth relationships have not been thoroughly evaluated under ongoing warming and aridification across the species' geographic distribution (Villalba et al. 1998; Reiter et al. 2024; Marcotti et al. 2021). This gap is especially relevant in ecotonal environments, where low precipitation, marked climatic seasonality, and shallow rocky soils with low water-holding capacity may amplify drought impacts on radial growth. Therefore, understanding how cumulative water stress and recent trends toward stronger multi-year moisture deficits contribute to sustained growth reduction is critical (Anderegg et al. 2015; González de Andrés et al. 2025).

To evaluate changes in *A. chilensis* growth in response to recently documented climate change, we developed millennial-length tree-ring chronologies by integrating samples from living trees with subfossil cross-sections. Three representative sites from the forest–steppe ecotone in northern Patagonia were sampled. This combined sampling strategy enabled the construction of long records that place recent growth variability within a robust long-term context. The specific objectives of this study were to: (a) characterize millennial-scale growth patterns of *A. chilensis* in northern Andean Patagonia; (b) evaluate radial growth responses during recent decades under exceptionally warm and dry conditions; and (c) assess the extent to which severe droughts, cumulative hydroclimatic stress, and post-drought persistence are associated with the extremely reduced growth observed in recent decades.

Our results highlight the recent decline of *Austrocedrus* growth under a progressively warmer and drier climate regime and underscore the likely importance of cumulative stress and drought legacy effects in shaping this reduction.

Materials and methods

The species

Austrocedrus chilensis is an endemic conifer in the southern Andes. In Argentina, its natural distribution forms a narrow belt along the eastern Andean slope, arranged in patches of variable size, with the southern sector showing the greatest extent and continuity (Fig. 1; Pastorino et al. 2015). At three sites on the eastern margin of the forest–steppe ecotone: Cuyín Manzano (40°43′ S, 71°07′ W), Confluencia Limay-Traful (40°44′ S, 71°02′ W), and Nahuel Pan (42°58′ S, 71°10′ W), where water availability is a key constraint on forest growth, the preservation of subfossil *A. chilensis* material is excellent. These sites have been investigated dendrochronologically for more than three decades and were selected to develop ring-width chronologies that combine increment cores from living trees with cross-sections from dead trees. Integrating these materials enables the construction of millennial-length records in northern Patagonia. Previous studies have documented the high sensitivity of these ecotonal *A. chilensis* forests to hydroclimatic variability (Villalba and Veblen 1997a, b, c; Villalba et al. 1998; Marcotti et al. 2025).

We observed that subfossil *A. chilensis* wood is best preserved at marginal growth microsites, such as rocky outcrops, where rapid post-rainfall drainage reduces wetting of dead stems and favors long-term wood conservation. These exposed microsites typically have shallow or absent soils and lower radial growth than adjacent, more protected patches with deeper soils and greater water retention (Table 1); in the latter, trees are larger, live crown percentage increases, and wood decomposition is more evident. In contrast, trees growing on rocky, drought-prone microsites tend to form a higher proportion of latewood, which enhances the durability of dead stems and increases the likelihood of finding very old subfossil material.

At Cuyín Manzano (Fig. 2a), the subfossil cross-section CUY261a (Fig. 2b, c) contains 786 rings along its longest radius (22 cm), spanning CE 178–963, with a mean radial increment of 0.28 mm yr^{-1}. The specimen was found exposed at the surface, with no evidence of substantial burial, in a geomorphic setting dominated by rocky outcrops and shallow soils (Fig. 2a), where dead wood preservation is particularly common.

Climate

Northern Patagonia has a cool-temperate climate marked by strong seasonal contrasts in temperature and precipitation. These contrasts are closely linked to the seasonal displacement and intensity of the Southern Hemisphere Westerlies, as well as to their modulation by broader patterns of Southern Hemisphere atmospheric circulation

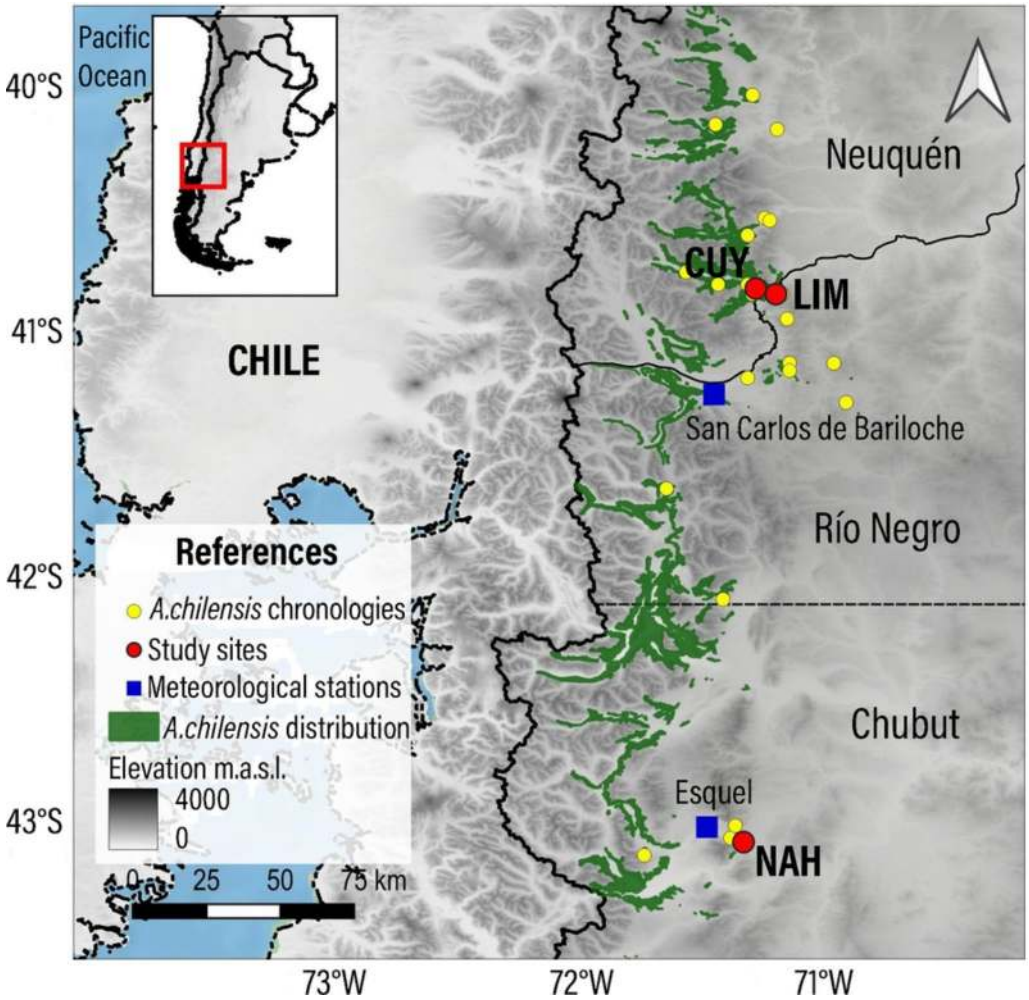


Fig. 1 Study area and sampling network of *Austrocedrus chilensis* in northern Patagonia, Argentina. The map shows the distribution of *A. chilensis* within the 40°–43.5° S latitudinal band (green shading; after Pastorino et al. 2015). Red circles mark the three study sites: Cuyín Manzano (CUY), Confluencia Limay-Traful (LIM), and Cerro Nahuel Pan (NAH), used to develop the millennial tree-ring records. Yellow circles indicate other existing *A. chilensis* tree-ring chronologies, and blue squares represent the meteorological stations whose temperature and precipitation records were used in this study. The grayscale background shows elevation (m a.s.l.). The geographic range of *A. chilensis* extends farther north than the area shown here

(Villalba et al. 2003; Garreaud et al. 2013). At Bariloche and Esquel, mean annual temperatures typically range between 8 and 10 °C, with cold winters and mild summers. During the austral summer (DJF), mean temperatures reach 14.0 °C in Bariloche and 14.4 °C in Esquel, whereas in winter (JJA) they drop to 2.9 °C and 2.7 °C, respectively (1914–2023 period). Precipitation is strongly concentrated in winter: cumulative totals during JJA reach 423 mm in Bariloche and 209 mm in Esquel, and June is the wettest month at both locations (161.5 mm in Bariloche and 80.3 mm in Esquel). In contrast, summer precipitation (DJF) declines to 78.3 mm in Bariloche and 61.5 mm in Esquel, reflecting the pronounced hydrological seasonality of the Andean Patagonian climate.

Superimposed on this seasonal cycle is a strong west-to-east precipitation gradient. Western sectors, more directly exposed to moist air masses from the Pacific Ocean, receive higher annual totals, whereas to the east, across interior valleys and plains, precipitation decreases sharply, resulting in relatively dry summers and high interannual variability (Masiokas et al. 2008; Hurtado et al. 2023). This spatial heterogeneity is further modulated by large-scale circulation modes such as the El Niño-Southern Oscillation (ENSO) and the Southern Annular Mode (SAM), whose positive phases have been associated with reduced precipitation and drier conditions in northern Patagonia, particularly

Table 1 Characteristics of sampled sites

Variable	Cuyín Manzano (CUY)	Confluencia Lim-Tra (LIM)	Cerro Nahuel Pan (NAH)	Regional (REG)
Latitude	40° 43′ S	40° 44′ S	42° 58′ S	-
Longitude	71° 07′ W	71° 02′ W	71° 10′ W	-
Elevation (m a.s.l.)	1030	950	990	-
Time span	178–2022	267–2022	1070–2018	178–2022
Time span (years)	1845	1756	949	1845
Number of dated series	462	479	438	1378
Series intercorrelation	0.60	0.59	0.59	0.55
Mean sensitivity	0.29	0.29	0.28	0.29
Mean tree age (years)	218.9	256.7	190.5	222.9
Mean RW (mm)	0.53	0.49	0.67	0.55
SD RW (mm)	0.31	0.27	0.36	0.31
EPS*	0.95	0.97	0.94	0.94
Rbar*	0.42	0.36	0.33	0.27
Living trees				
Time span	1464–2022	1461–2022	1517–2018	-
Mean sensitivity	0.28	0.30	0.27	-
Mean RW (mm)	0.63	0.62	0.81	-
SD RW (mm)	0.41	0.35	0.43	-
Subfossil wood				
Time span	178–1990	267–1981	1070–2006	-
Mean sensitivity	0.30	0.28	0.28	-
Mean RW (mm)	0.41	0.43	0.55	-
SD RW (mm)	0.23	0.23	0.30	-

* Calculated on standardized ring-width values for the periods 700–2022 (CUY), 900–2022 (LIM), 1200–2018 (NAH) and 520–2022 (REG)

during the warm season (Garreaud et al. 2009; Villalba et al. 2012; Hurtado et al. 2023).

Assessment of recent climate variations

To characterize recent hydroclimatic variability in the study region, we used monthly temperature and precipitation records from the Bariloche and Esquel meteorological stations (Fig. 1). Both stations are located near the *A. chilensis* sampling sites and provide the longest and most complete instrumental records available for northern Patagonia. To infill remaining data gaps and extend the instrumental series as far back as possible, we also incorporated historical monthly temperature and precipitation data for each station. These historical records were obtained from the Argentine National Meteorological Service and from CENPAT-CONICET (Puerto Madryn, Chubut) and were used to complement station data available through international repositories (NASA GISS; KNMI). This procedure extended the temperature records back to 1914 for Bariloche and 1913 for Esquel, and the precipitation records back to 1916 for both stations.

To characterize low-frequency regional variability and facilitate comparisons between Bariloche and Esquel, we computed standardized monthly temperature anomalies using a common reference period (1975–2024). For each calendar month, standardized anomalies were calculated by subtracting the reference-period monthly mean from each observation and dividing by the corresponding reference-period standard deviation. This transformation expresses temperature variability in dimensionless units and is widely used in climatology to analyze variability and extremes (von Storch and Zwiers 1999; Wilks 2011).

To identify shifts in the regional thermal regime, we applied structural breakpoint analyses to the Bariloche and Esquel temperature series using the strucchange package in R (Zeileis et al. 2002), following the least-squares framework of Bai and Perron (1998, 2003). Breakpoints were tested as changes in the mean level of the series (intercept-only models, without covariates) and were fitted to both monthly series and annual aggregates. Candidate partitions for different numbers of segments were evaluated by minimizing the residual sum of squares (RSS), and the optimal number of breakpoints

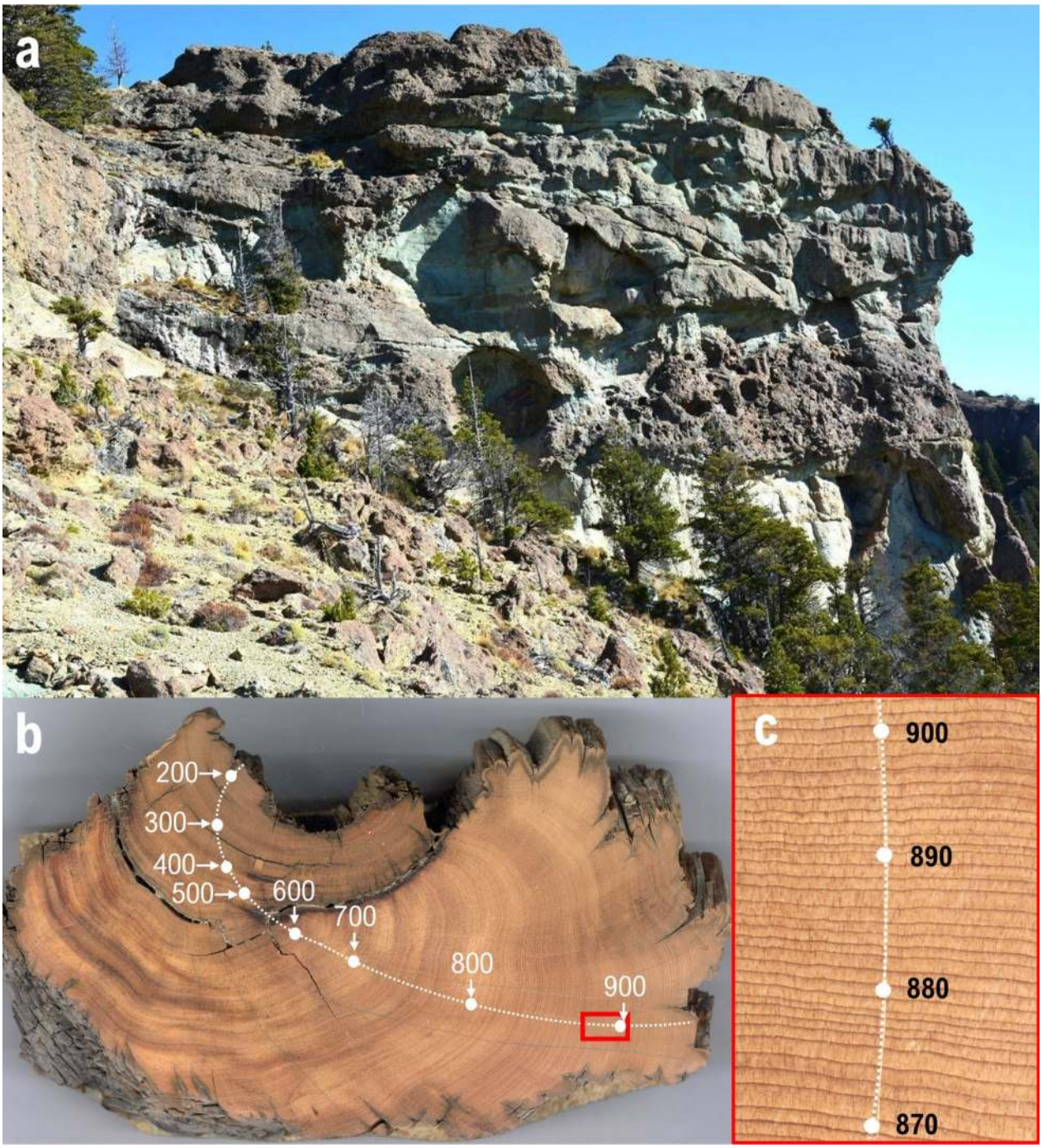


Fig. 2 Subfossil wood preservation at the Cuyín Manzano site (CUY). **a** Rocky outcrop at the Cuyín Manzano site (CUY), where abundant coarse rock fragments and shallow sandy soils constrain the growth of *A. chilensis*. **b** Cross-section CUY261a, which contains 786 rings spanning CE 178–963. This sample has remained exposed at the surface since tree death, most likely for more than 1000 years. In microsites where microrelief promotes greater soil water retention, tree growth is faster, woody material decomposes more rapidly, and the probability of preserving very old wood is lower. **c** Enlarged detail of cross-section CUY261a showing the identification of annual rings for the interval CE 871–902

was selected using the Bayesian Information Criterion (BIC; Schwarz 1978).

Because precipitation distributions are often strongly skewed and non-normal, we analyzed accumulated seasonal totals rather than standardized monthly anomalies. This approach preserves the hydrological magnitude of events and avoids potential distortions associated with directly standardizing strongly skewed distributions (Lloyd-Hughes and Saunders 2002). We identified dry summers using a percentile-based threshold: a "dry summer" was defined as any summer in which accumulated December–February precipitation fell below the 10th percentile (P10) of the distribution. This non-parametric approach is commonly used to characterize dry extremes and their recurrence (McKee et al. 1993; Lloyd-Hughes and Saunders 2002). The frequency of dry summers was computed as the number of P10 events within a centered 11-year moving window to highlight low-frequency variability and trends in drought recurrence. Potential abrupt changes in drought recurrence were assessed using the non-parametric Pettitt test (Pettitt 1979).

To assess drought severity, intensity, and duration, we used the Standardized Precipitation Evapotranspiration Index (SPEI) from the global SPEIbase v2.10 dataset (Reig-Gracia et al. 2023). SPEI is a multi-scalar drought index based on the climatic water balance (precipitation minus potential evapotranspiration), capturing both water supply and atmospheric demand. We accessed SPEI through Google Earth Engine using the CSIC/SPEI/2_10 collection. The dataset provides monthly SPEI at 0.5° spatial resolution and at accumulation timescales from 1 to 48 months. In this product, potential evapotranspiration is estimated using the FAO-56 Penman–Monteith method (Vicente-Serrano et al. 2010; Reig-Gracia et al. 2023). SPEI time series were extracted as point values using the coordinates of the dendrochronological sites (Cuyín Manzano/Confluencia Limay-Traful and Cerro de Nahuel Pan). We evaluated 12-, 24-, 36-, and 48-month timescales ending in February to represent hydroclimatic conditions at the end of the austral summer.

Development of ring-width chronologies

Although dendrochronological research in northern Patagonia began more than 70 years ago (Schulman 1956; LaMarche et al. 1979; Boninsegna et al. 2009), field campaigns specifically targeting millennial-length *Austrocedrus chilensis* ring-width chronologies were conducted since 2015 at sites where subfossil wood is relatively abundant (Fig. 2). At each site, we sampled dominant and co-dominant living trees, avoiding individuals with visible disturbances (e.g. fire scars) or extensive crown dieback (> 75% dead crown). We extracted at least two 5-mm increment cores per tree using Pressler borers at ~ 1.3 m height. From dead stems, we collected cross-sections from the widest portion of the bole using a chainsaw. This design combined living-tree records spanning the last ~ 300–400 years with subfossil material capable of extending site chronologies through the last millennium and beyond (Table 1).

The millennial chronologies also incorporated earlier collections from living trees and remnant wood obtained during earlier sampling campaigns (Fig. S1). The earliest collections from Cuyín Manzano and Nahuel Pan (referred to as Estancia Teresa in LaMarche et al. 1979) were coordinated by Richard Holmes in 1970 at the Tree-Ring Laboratory, University of Arizona. These sites, together with the Confluencia Limay-Traful area included in the present study, were resampled in 1989–1992 (Villalba and Veblen 1997a, b) and more recently in 2012–2014 (Marcotti et al. 2025).

In the laboratory, increment cores were mounted on grooved wooden holders and cross-sections were secured to wooden boards; all samples were progressively sanded with increasingly fine sandpaper until ring boundaries were clearly visible. Samples were visually crossdated following standard procedures (Stokes and Smiley 1968). Following Schulman's (1956) Southern Hemisphere convention, rings were assigned to the year in which growth began. Ring widths were measured to 0.001 mm using a Velmex UniSlide measuring system coupled to a computer. A subset of samples was scanned at high resolution (A3 scanner) and measured on digital images using CooRecorder/CDendro (Larsson 2010), following Maxwell et al. (2021) recommendations for measurement and quality control. Agreement between visual and image-based crossdating was evaluated through the program COFECHA (Holmes 1983).

To extend the chronologies, subfossil cross-sections were incorporated stepwise. First, subfossil samples were crossdated against living-tree site chronologies using diagnostic years and statistical concordance. As the master chronology lengthened, progressively older subfossil pieces were dated against the extended record, enabling incremental back-extension at sites with sufficient material. Sampling effort, temporal coverage, overlap among segments, and site-specific quality metrics are reported in Table 1. Chronology quality and reliability were assessed using standard dendrochronological statistics, including Rbar, expressed population signal (EPS), and mean sensitivity (MS) (Wigley et al. 1984; Briffa 1990). Inferences were restricted to intervals with adequate common signal (EPS ≥ 0.85) and sufficient annual replication (N ≥ 10 series year^{-1}); statistical analyses were conducted only when these criteria were met.

Assessment of recent growth trends

Long-term growth patterns can be influenced by (i) large differences between trees in ring width and (ii) the expected age-related decline in ring width as trees grow older (i.e. the biological growth trend). To reduce the influence of series with exceptionally low or high mean growth rates, each series was divided by its mean ("horizontal line through the mean", ARSTAN option 6), so that all trees contributed comparable weight to the final chronology. Under this standardization, any persistent decline in the resulting chronologies would indicate that the trend is not simply an artifact of among-tree differences in growth rate.

To assess whether progressive aging of the sampled trees could contribute to recent growth trends, we evaluated (i) changes in the mean cambial age of contributing series during the period of interest (e.g. the last three decades) using the ARSTAN mean-age statistic (Cook and Krusic 2005), and (ii) the expected magnitude of age-related changes in radial increment at ages comparable to those represented in recent decades. For this purpose, all series contributing to each chronology were aligned by cambial age and averaged to estimate a regional growth curve, which was then used to quantify the fraction of recent ring-width change potentially attributable to increasing age.

Recent growth trends and standardization

Ring-width series are standardized to remove non-climatic trends related to tree age and size, as well as growth changes associated with competition and/or disturbance (Fritts 1976; Cook and Kairiukstis 1990). Some detrending approaches can introduce the "increasing-end" problem, generating spurious positive trends near the end of standardized series (Cook et al. 1995). Because this artifact could bias inference about the magnitude of recent growth reductions in *A. chilensis*, we assessed the sensitivity of recent trends to alternative standardization choices. Original ring-width series were standardized in ARSTANv49 (Cook and Krusic 2005) using multiple options, including negative exponential curves (NEC), age-dependent splines (ADS), median filtering with sharpening/smoothing routines (MFSS), and Regional Curve Standardization (RCS) (Briffa and Melvin 2011), among others. In addition, we implemented Signal-Free standardization (Melvin and Briffa 2008) using both NEC and RCS detrending options. Finally, the chronologies developed using different standardization options were compared with each other to select those that best reflected the growth patterns observed in the raw series or in the series standardized using the "horizontal line through the mean" option.

Growth patterns during recent decades

To characterize growth anomalies in recent decades, we computed overlapping 10-year moving means of the growth indices, restricting analyses to chronology intervals with adequate signal strength (EPS > 0.85): from CE 700 onward at Cuyín Manzano, CE 900 onward at Confluencia Limay-Traful, and CE 1200 onward at Cerro Nahuel Pan. Decadal means were calculated with 10-year windows shifted by one year. For each site, we built the distribution of all complete decadal means and quantified recent anomalies by comparing the 1998–2022 period (Cuyín Manzano and Confluencia Limay-Traful) and 1998–2018 (Nahuel Pan) against their respective long-term distributions. This comparison period was motivated by precipitation breakpoint analyses indicating an increased frequency of severe summer (JFM) droughts at both Bariloche and Esquel since the summer 1997 (Fig. 3).

To test whether the recent low-growth episode is unprecedented in the long-term record, we analyzed the regional chronology (CE 523–2022; $n = 1500$; EPS > 0.85) using complementary metrics of extremeness, persistence, and significance under temporal dependence. First, as for individual sites, we computed overlapping, right-aligned 10-year moving means of the annual series (each decadal mean assigned to the final year of the window). Using the distribution of complete decadal windows, we defined a low-growth threshold as the 5th percentile (P5 = 0.78) and located recent windows using empirical percentiles and tail probabilities. Because overlapping windows induce serial dependence, we also constructed non-overlapping decades anchored at 2022 (2013–2022, 2003–2012, …, 523–532; 150 complete decades) and evaluated recent decades against that historical distribution (Wilks 2011). Finally, to obtain robust p-values under autocorrelation, we implemented a circular block bootstrap on the regional chronology (stationary null preserving serial dependence), resampling fixed-length circular blocks ($L = 10$, 20, 30, 50 years; $B = 2000$ replicates per L) and recomputing (i) whether the segment equivalent to 1998–2022 yields 25/25 decadal means ≤ P5 (persistence), and (ii) whether the segment minimum is at least as low as observed (Künsch 1989; Politis and Romano 1992; Lahiri 2003; Mudelsee 2010).

Relationships between climate and tree growth

The extreme climatic changes documented in northwestern Patagonia provide a plausible environmental explanation for the reduced radial growth of *A. chilensis* in recent decades. To evaluate this hypothesis, we compared the regional growth chronology (integrating the three millennial chronologies) with instrumental temperature and precipitation records from the Bariloche and

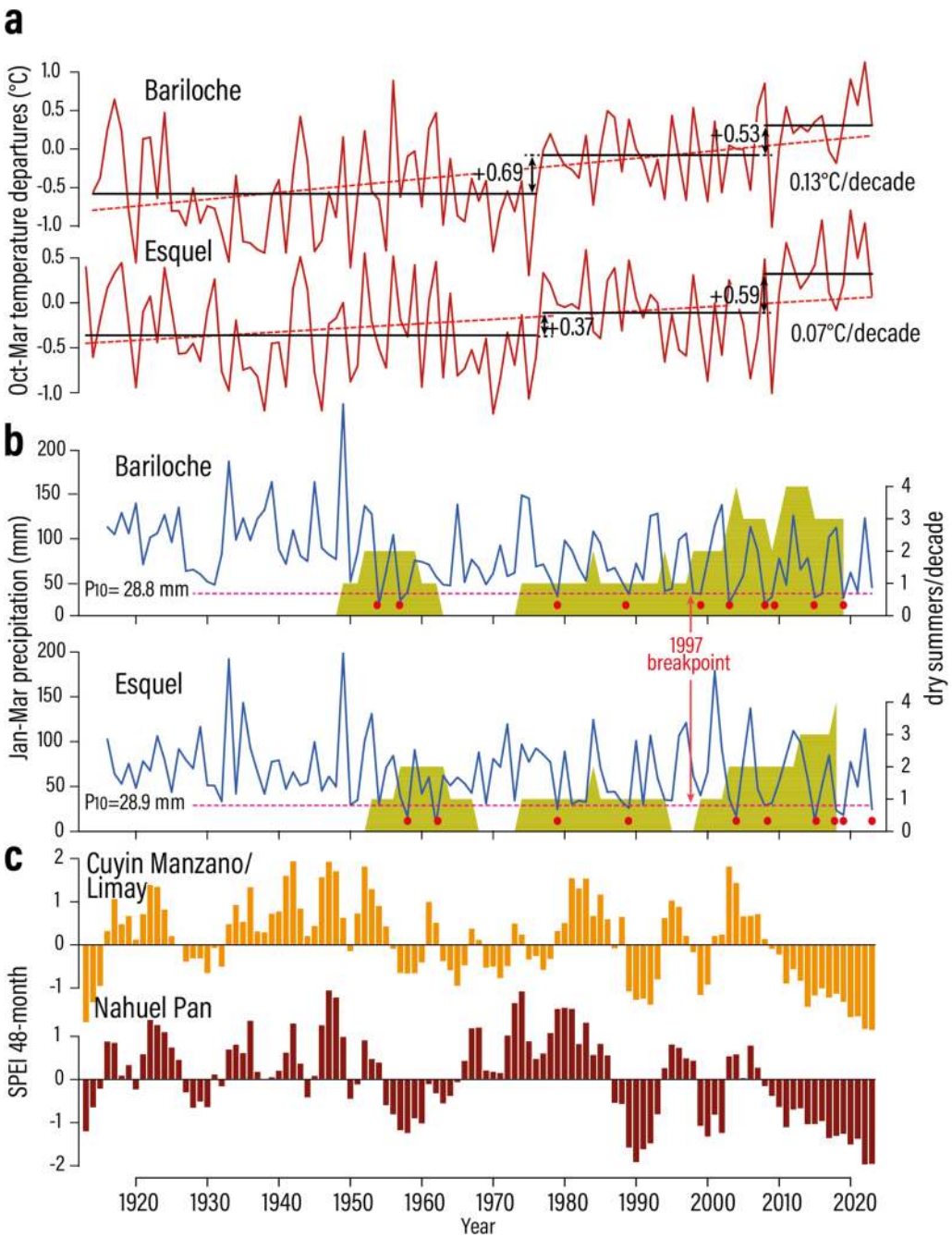


Fig. 3 Climate variability in the eastern sector of the northern Patagonian Andes. **a** Interannual October–March temperature variability (solid lines), linear trends for the full period (red dashed lines), and regime means for 1914–1976, 1977–2007, and 2008–2022 (black horizontal lines) at the Bariloche and Esquel meteorological stations. **b** Summer accumulated precipitation (January–March) for 1916–2024. The left axis shows seasonal precipitation totals, whereas the right axis shows the frequency of dry summers, computed as an 11-year moving mean of the number of events with precipitation below the 10th percentile of each series (P10). Red circles denote summer precipitation values below P10. The vertical line marks the breakpoint in precipitation identified using the Pettitt (1979) test. **c** Time series of the 48-month Standardized Precipitation-Evapotranspiration Index (SPEI48) ending in February of the current growing season for the Cuyín Manzano/Limay-Traful and Cerro Nahuel Pan sites over the period 1913–2023

Esquel meteorological stations. Monthly climate series were aggregated into seasonally relevant predictors based on the species' phenology and prior dendroclimatic evidence. Growing-season temperature was defined as mean October(t–1)–March(t) temperature, matching the main period of cambial activity. Hydrological-year precipitation was calculated as total May(t–1)–April(t) precipitation. To derive regional predictors, monthly series from both Bariloche and Esquel stations were standardized as z-scores over the 1913–2022 reference period and then averaged, yielding regional temperature and precipitation series.

In a first step, the temperature and precipitation seasonal variables were used as predictors in linear regression models to quantify the fraction of *A. chilensis* growth variance explained by regional climate variability (Fritts 1976; Villalba et al. 1998). Because a combined water-stress metric may better capture growth responses than temperature or precipitation alone, we also evaluated SPEI at 12-, 24-, 36-, and 48-month timescales as predictors of radial growth over the last century (Vicente-Serrano et al. 2010).

Since model fit deteriorated during the last three decades, we implemented a second step to test for non-stationarity in the climate–growth relationship. Models were calibrated over 1913–1997 and then applied, without recalibration to estimate expected growth during the recent period 1994–2022. Annual residuals (Res_ann) were defined as observed minus predicted growth and interpreted as the component of variability not explained by contemporaneous climate under the historical climate–growth relationship.

To quantify compounded regional hydroclimatic stress and its persistence, we combined spring–summer temperature and annual precipitation into a Standardized Dryness Index (SDI). For each year, temperature was computed as mean October($t-1$)–March(t) temperature, and precipitation as total May($t-1$)–April(t) precipitation, both aligned with the dendrochronological growth year t, for Bariloche and Esquel. Temperature and precipitation were standardized as z-scores relative to the 1913–1997 reference period, and station-level z-scores were averaged to obtain regional temperature and precipitation series. The annual index was defined as $\mathrm{SDI}_t = -z + z\mathrm{T}_t$, so that higher values indicate greater hydroclimatic stress associated with warmer and/or drier conditions. To capture potential drought legacy effects, we calculated SDI_prev5 as the mean SDI over the previous five years, from t–1 to t–5, representing accumulated hydroclimatic stress preceding the growth year. We evaluated whether residuals became more negative under greater antecedent stress using two complementary approaches for the period 1994–2022. First, we assessed the relationship between Res_ann and SDI_prev5 using linear regression with Heteroskedasticity- and Autocorrelation-Consistent errors (HAC(1)) (Newey and West 1987). This correction leaves coefficient estimates unchanged but adjusts standard errors, t statistics, and p values to account for non-constant error variance and serial correlation between adjacent residuals. Second, we defined an antecedent-stress threshold (τ) as the 80th percentile of SDI_prev5 during 1913–1997 and compared mean residuals between regimes (low vs. high antecedent stress). Finally, to visualize potential nonlinearities in the climate–tree growth relationship, we binned SDI_prev5 into quintiles (Q1–Q5) for 1994–2022 and computed the mean residual within each quintile.

Assessment of drought legacy effects

We used Superposed Epoch Analysis (SEA) to quantify the mean growth (or residual) response to drought years and to test whether drought effects persisted beyond the event year itself ("legacy effects") (Kannenberg et al. 2019; Rao et al. 2019). For each drought event year (t_0), we extracted anomalies over lag windows relative to t_0 using two complementary response variables: (i) growth anomalies from the regional chronology and (ii) residual anomalies delivered from the baseline climate–growth model. Both variables were standardized as z-scores relative to the pre-decoupling baseline period 1917–1997.

Drought events were defined a priori from an independent precipitation-based analysis of major regional drought years. To avoid treating consecutive drought years as independent events, multi-year episodes were declustered so that only non-consecutive event years were retained in the SEA. Events were then stratified into pre-1994 and post-1994 groups to align the SEA comparison with the onset of systematic negative residual departures in the climate–growth relationship during the mid-1990s. The pre-1994 group included 1958, 1962, 1979, and 1989 ($n=4$), whereas the post-1994 group included 1999, 2004, 2008, 2015, and 2019 ($n=5$).

For the residual-based SEA, annual residuals were calculated as observed minus predicted growth from a baseline climate–growth model (regional chronology $\sim z\mathrm{P} + z\mathrm{T}$) calibrated over 1917–1997. This approach allowed us to evaluate whether post-drought growth suppression exceeded expectations from the historical climate–growth relationship.

Composite mean anomalies at each lag were computed by averaging across events within each period. To quantify drought legacy effects, we defined a persistence metric as the mean anomaly over post-drought years $t+1$ to $t+5$ and $t+1$ to $t+7$, depending on data availability. To test whether persistence differed between pre-1994 and post-1994 events, we used a one-sided permutation test

comparing the mean persistence metric between groups, with the alternative hypothesis that post-1994 events were more negative than pre-1994 events (Good 2005). This approach is robust for small event sample sizes and makes minimal distributional assumptions. For visualization, we also derived bootstrap confidence bands for the composite SEA curves by resampling events with replacement (Efron and Tibshirani 1993; Rao et al. 2019). Because the record ends in 2022, sample size decreased at longer positive lags for the most recent drought events.

Results

Recent hydroclimatic change in northern Andean Patagonia

Instrumental records from northern Andean Patagonia show sustained warm-season warming, a marked increase in the frequency of extreme summer droughts, and persistent multi-year moisture deficits during recent decades. October–March temperatures, the seasonal window most directly related to the growth of *A. chilensis*, show a clear long-term warming trend. Linear trends for 1914–2024 indicate increases of 0.13 °C per decade in Bariloche and 0.07 °C per decade in Esquel (Fig. 3a), with the stronger warming trend recorded at the northern site.

Breakpoint analyses of October–March temperatures, based on multiple change-point regression models, identified three climatically distinct periods at both meteorological stations: 1914–1976, 1977–2007, and 2008–2022 (Fig. 3a). In Bariloche, mean October–March temperatures increased by 0.69 °C in 1977 and by 0.53 °C in 2008. Esquel showed a similar pattern, with increases of 0.37 °C and 0.59 °C in the same years. The post-2007 period was characterized by the highest mean temperatures and the persistence of positive warm-season thermal anomalies (Fig. 3a).

Changes in precipitation reinforce this warming signal. January–March precipitation in Bariloche and Esquel reveals a pronounced increase in the frequency of extreme summer droughts during the late twentieth and early twenty-first centuries. Using the 10th-percentile threshold for each series (28.8 and 28.9 mm in Bariloche and Esquel, respectively), the non-parametric Pettitt test identified a significant breakpoint around 1997 in the recurrence of dry summers (Pettitt 1979). In Esquel, the proportion of extremely dry summers increased from 4.9% during 1916–1997 to 23.1% during 1998–2023, whereas in Bariloche it rose from 4.9% to 26.9% over the same intervals (Fig. 3b). These results indicate that extreme summer droughts have become substantially more frequent across northern Andean Patagonia in recent decades.

This recent drying trend is also evident in multi-year hydroclimatic conditions. February SPEI48 shows predominantly negative values at all study sites in recent decades (Fig. 3c). Since approximately 2009, SPEI48 has remained persistently negative at Cuyín Manzano, Confluencia Limay-Traful, and Nahuel Pan, indicating sustained regional moisture deficits. The most recent dry interval spans 14 consecutive years with negative SPEI48 values, making it the longest episode of persistent multi-year drought within the instrumental record (Fig. 3c).

Millennial tree-ring chronologies

The new ring-width chronologies developed for *A. chilensis* at the forest–steppe ecotone in northern Patagonia show adequate replication and strong internal coherence. The three records span long time intervals, reaching nearly 1850 years in length, and maintain annual replication above 10 series from CE 1004 at CUY, CE 764 at LIM, and CE 1244 at NAH (Table 1). Mean interseries correlation is similar among sites, with values close to 0.60, indicating a strong common signal in radial growth. Mean sensitivity ranges from 0.27 to 0.29, reflecting moderate interannual variability in growth. The mean age of trees included in the chronologies differs among sites, with the oldest trees at LIM, intermediate ages at CUY, and the youngest at NAH (Table 1). Chronology robustness, evaluated using the Expressed Population Signal (EPS), indicates that the records provide reliable estimates of the common growth signal for approximately the last millennium, although the timing of robust signal strength varies among sites.

Chronologies based exclusively on living trees cover broadly similar periods across the three sites. Within this subset, mean sensitivity is also comparable among sites, averaging 0.28. Mean ring width (RW) is similar at CUY (0.63 mm) and LIM (0.62 mm), whereas NAH shows higher values (0.81 mm). The standard deviation of RW is similar across sites, indicating comparable levels of absolute growth variability. For all three sites, EPS in the living-tree chronologies remains above 0.85 over the last four centuries.

Recent growth decline, chronology age structure and standardization

Figure 4 shows the mean chronologies for Cuyín Manzano, Confluencia Limay-Traful, and Cerro Nahuel Pan derived from averaging ring-width measurements from living trees. Mean ring width at each site fluctuated around 0.6 mm yr^{-1} over the last 300 years. The common growth signal at each site, assessed using EPS, remained during the last three centuries consistently above the conventional reliability threshold (EPS > 0.85), supporting the robustness of inter-site comparisons. Although the number of series contributing to the mean varied through time, particularly increasing from 1850 onward,

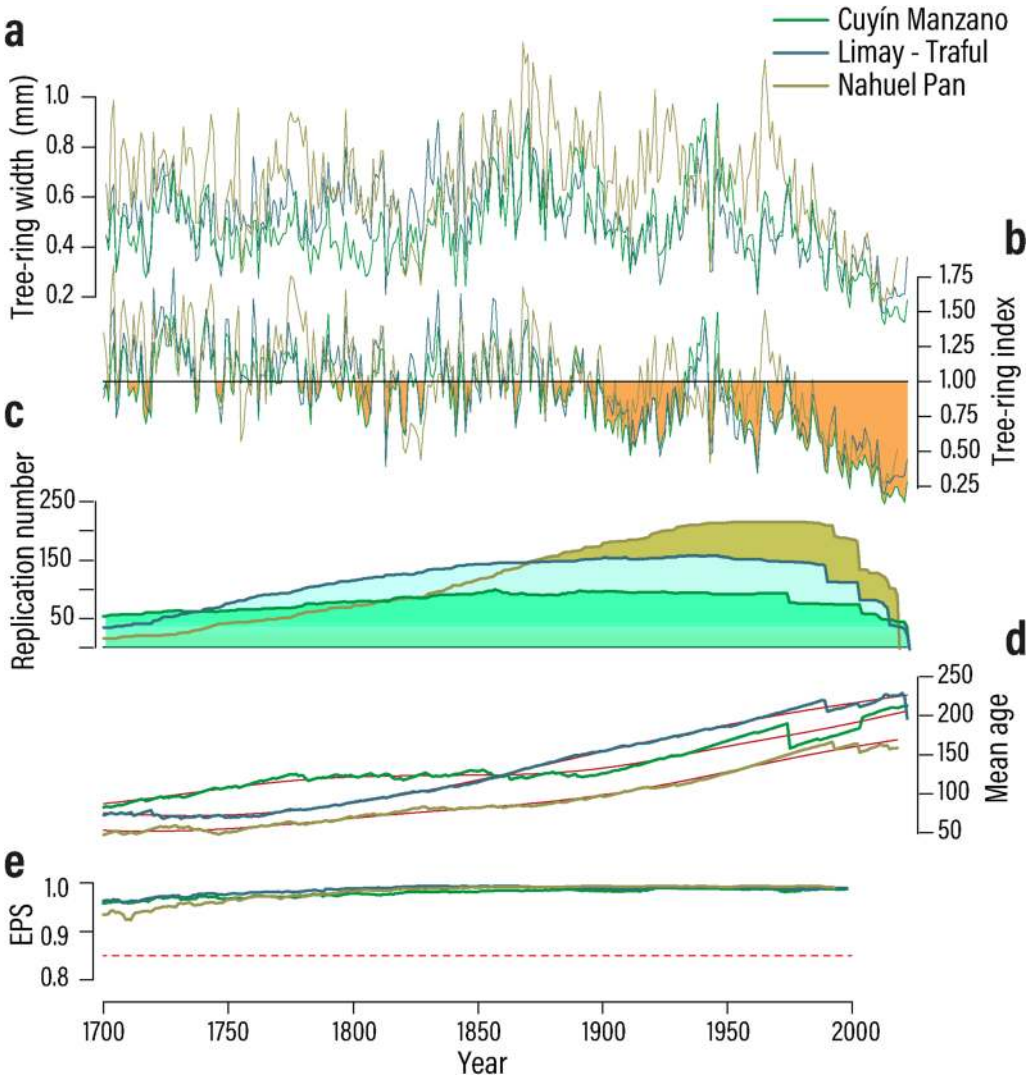


Fig. 4 Characteristics of the *A. chilensis* ring-width chronologies based on living trees at the three study sites: **a** raw ring-width series (RW), **b** standardized chronologies, **c** number of increment-core series (*n*), **d** mean age of sampled living trees and **e** the Expressed Population Signal (EPS), estimated with ARSTAN v49 (Cook and Krusic 2005)

raw growth remained relatively stable (approximately 0.4–0.8 mm yr^{-1}) between 1700 and 1960–70. Thereafter, a pronounced decline in ring width began in the 1970s, reducing mean growth to $\leq$0.4 mm yr^{-1} and to even lower values during the two most recent decades (Fig. 4a).

Although the decline in *A. chilensis* radial growth since the mid-1970s could hypothetically reflect differences in absolute growth rates among individuals or narrower rings associated with increasing tree age, a first standardization approach based on a horizontal mean line (Fig. 4b) still indicates that the recent decline is unprecedented within the well-replicated portion over the last three centuries (Fig. 4). This result indicates that the recent decline remains evident after accounting for differences in absolute growth rates among the trees included in the chronologies.

In a second step, we evaluated whether the reduced growth observed in recent decades, after accounting for differences in individual growth rates, could instead be explained by increasing tree age over the last 30–40 years. At Cuyín Manzano, mean tree age during 1993–2022 varied approximately between 174 and 212 years, implying an age-related reduction in mean ring width of about 0.035 mm over this interval, based on the expected change associated with increasing age from 174 to 212 years (Fig. S2a). Over the same period, however, the observed decline in the CUY raw ring-width

chronology was 0.105 mm, estimated as the difference in mean growth between the five-year intervals 1993–1997 and 2018–2022 (Fig. 4a). At Confluencia Limay-Traful, cambial age ranged between 208 and 230 years during 1993–2022 (Fig. S2b), corresponding to an age-related reduction of 0.026 mm, whereas the observed decline in mean raw growth was 0.120 mm. Finally, at Nahuel Pan, cambial age over 1989–2018 ranged from 158 to 162 years (Fig. S2c), yielding an expected age-related reduction of only 0.008 mm; in contrast, the observed decline in raw growth between 1989–1993 and 2014–2018 was 0.239 mm. Overall, these comparisons show that the decline observed in raw ring-width series during the last three to four decades was approximately three to six times greater than expected from increasing cambial age alone.

Reduced recent growth and standardization

Having shown that recent radial growth decline in *A. chilensis* is real, we then selected a standardization approach that minimizes variation in ring width associated with cambial aging (biological trend) and disturbance history, while preserving medium- to low-frequency variability relevant to the recent decline.

Figure 5 compares the Cuyín Manzano chronology developed using four alternative standardization methods. Overall, RCS and GNEC preserved the negative growth trend in recent decades more effectively than the other approaches. However, relative to the alternative methods, RCS amplified the interval of high growth during the mid-twentieth century and markedly depressed growth during the eighteenth century (Fig. 5), indicating a stronger reshaping of low-frequency variability. Comparable patterns were observed when the LIM and NAH records were standardized using the same detrending approaches (Figs. S3 and S4). Based on these comparisons, we selected the GNEC chronology for subsequent analyses.

Recent low growth is exceptional in the 1800-year record

The millennial-length chronologies developed from the combination of samples from living trees and dead/subfossil wood at Cuyín Manzano, Confluencia Limay-Traful, and Cerro Nahuel Pan (Fig. 6) span CE 178–2022, CE 279–2022, and CE 1070–2018, respectively.

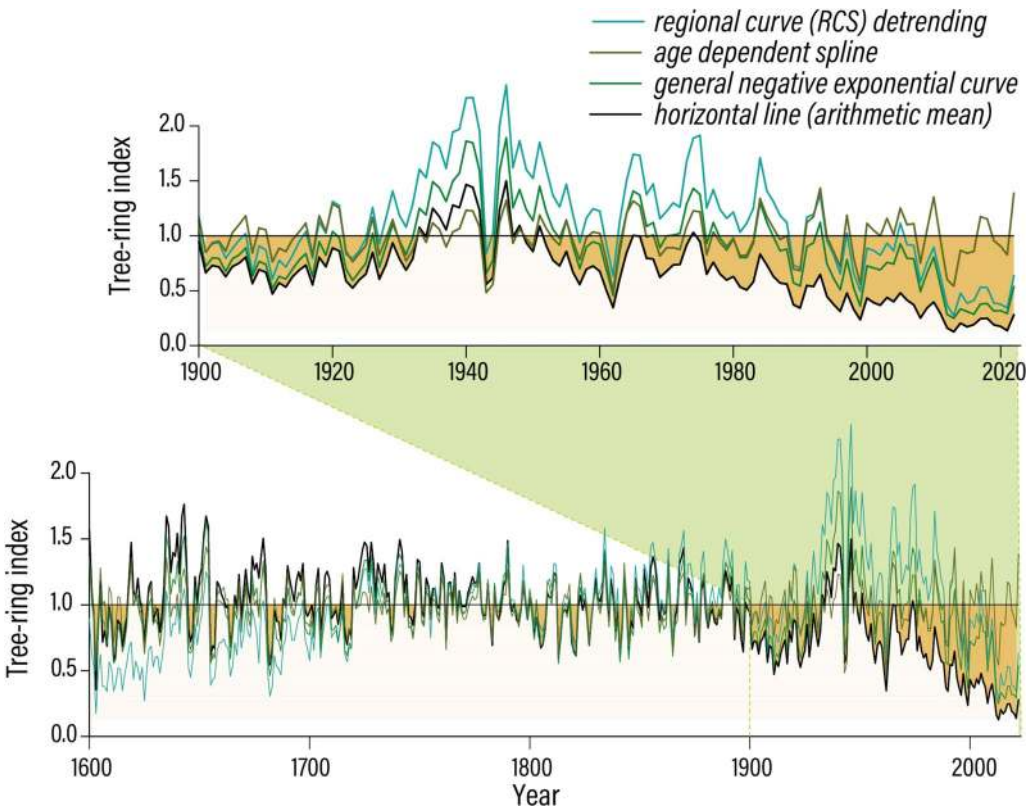


Fig. 5 Standardized chronologies for Cuyín Manzano (CUY) derived from four detrending methods applied to the original *A. chilensis* ring-width series. Methods include the horizontal transformation based on the mean ring width of each series, the Generalized Negative Exponential Curve, the Age-Dependent Spline, and Regional Curve Standardization, as implemented in ARSTAN v49 (Cook and Krusic 2005)

According to the Expressed Population Signal (EPS), the records reach adequate levels of population signal (EPS ≥ 0.85) from approximately CE 700 at Cuyín Manzano, CE 900 at Confluencia Limay-Traful, and CE 1200 at Cerro Nahuel Pan. Detailed dendrochronological statistics for each site are presented in Table 1. The composite regional chronology, constructed by integrating the three site chronologies, reaches the EPS ≥ 0.85 threshold back to approximately CE 520, thereby extending the analysis with robust signal over a broader temporal interval.

At interannual to multidecadal timescales, the three chronologies show partially synchronous patterns of variability during their statistically reliable common period (EPS ≥ 0.85). In all cases, the standardized indices show a marked decline in recent decades relative to most of the interval covered by records with adequate population signal (Fig. 6). This recent reduction is evident in each of the three site chronologies and is therefore also expressed in the composite regional chronology.

Analyses of decadal mean growth reveal that the recent decline is not only severe, but historically exceptional in magnitude and persistence across the study sites. Several of the lowest-growth decades of the entire record occur during the late twentieth and early twenty-first centuries (Table S1). Throughout this section, results are presented separately for overlapping decadal windows (10-year windows lagged by 1 year) and non-overlapping decades, which provide complementary perspectives on the magnitude and persistence of recent low-growth conditions (Fig. 7). Although the distributions are generally unimodal, they depart from normality and show asymmetric tails.

At Cuyín Manzano (Fig. 7a), post-2000 overlapping decadal windows fall within the extreme lower tail of the distribution, and the most recent intervals reach the absolute minimum in the moving-window analysis. The non-overlapping decades ending in 2022 lead to the same inference, with the most recent decade representing the lowest value in that independent decadal sequence. No other interval in the 1300-year chronology shows comparably low growth. These extreme values are also unusually persistent, forming extended runs of consecutive decadal windows below the 5th (P5) and 1st (P1) percentile thresholds defined from CE 700 onward. In particular, the 1998–2018 interval appears as a pronounced and nearly continuous run below the 5th percentile in the overlapping-window analysis. This sustained concentration of values in the lower tail has no clear counterpart elsewhere in the record, or only comparable values over much shorter periods.

At Confluencia Limay-Traful, the distribution of decadal means is also unimodal and somewhat more symmetric than at Cuyín Manzano, although it still departs from normality and shows a slight positive skew (skewness = +0.103). As at Cuyín Manzano, the most recent overlapping decadal windows show an exceptionally strong decline. The last 10–15 moving decadal windows fall within approximately the lowest 0.4% of the statistically reliable record since CE 700, indicating decadal growth conditions without precedent over this interval. In contrast to Cuyín Manzano, however, a marked shift is evident between the late 1990s–early 2000s and the post-2010 period. Decadal windows ending in 1998–2007 still show mean values around 0.84–0.80, well within the main body of the distribution, but are followed by a transition toward markedly lower values, culminating in the extreme minima of the 2010s and early 2020s.

At Nahuel Pan, the overlapping decadal window 2008–2017 constitutes the absolute minimum of the last 800 years (mean = 0.445; percentile ≈ 0.12%; *p*_low ≈ 0.001), marking the lowest decadal growth level for the 1200–2018 interval. As in the northern *A. chilensis* sites, the defining feature of the recent decline is its persistence: several consecutive post-1997 decadal windows fall within extreme percentiles ($p < 0.001$). Although overlapping decadal windows are not statistically independent, the analysis based on non-overlapping decades leads to the same conclusion: the decade 2009–2018 (mean = 0.493 mm) is the lowest among all non-overlapping decades.

The regional chronology confirms these site-level patterns and reveals an exceptionally persistent modern low-growth regime. In the overlapping decadal series, all 25 decadal windows ending in 1998–2022 fall at or below the 5th percentile (P5) threshold, and the segment minimum reaches 0.405 mm, placing this recent interval in the extreme lower tail of the historical distribution

(See figure on next page.)

Fig. 6 Millennial-length *A. chilensis* ring-width chronologies developed at the forest–steppe ecotone of northern Patagonia, on the eastern side of the Andes. The records combine samples from living trees and dead/subfossil wood from **a** Cuyín Manzano, **b** Confluencia Limay-Traful, and **c** Cerro Nahuel Pan; these site chronologies were subsequently combined into a **d** regional chronology. Each panel shows the standardized ring-width index obtained after detrending individual series with a Generalized Negative Exponential Curve (GNEC) (thin line), along with a 32-year cubic smoothing spline (thick line). Interannual variations in EPS, calculated in 50-year moving windows with a 1-year lag, are shown below each chronology

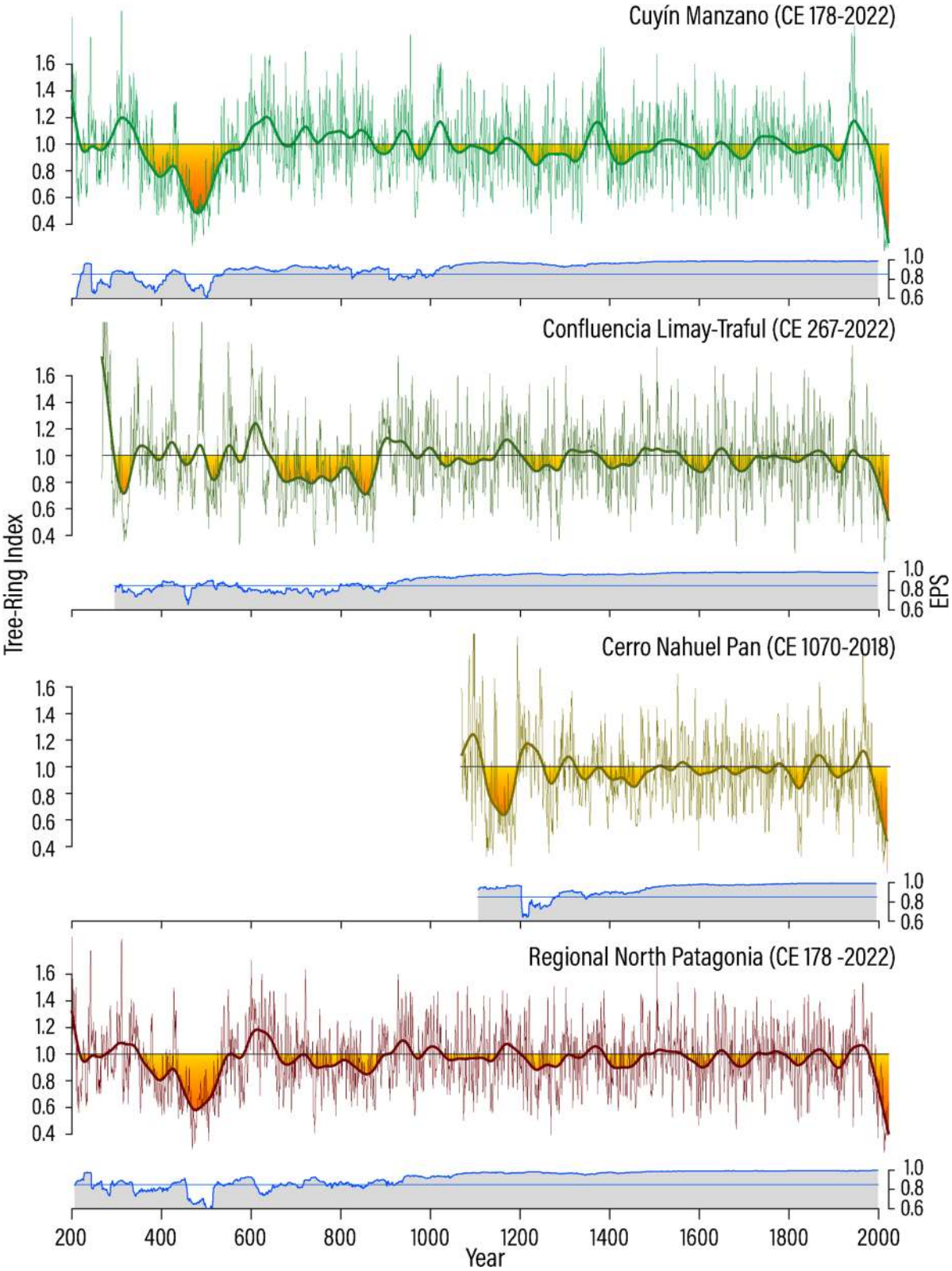


Fig. 6 (See legend on previous page.)

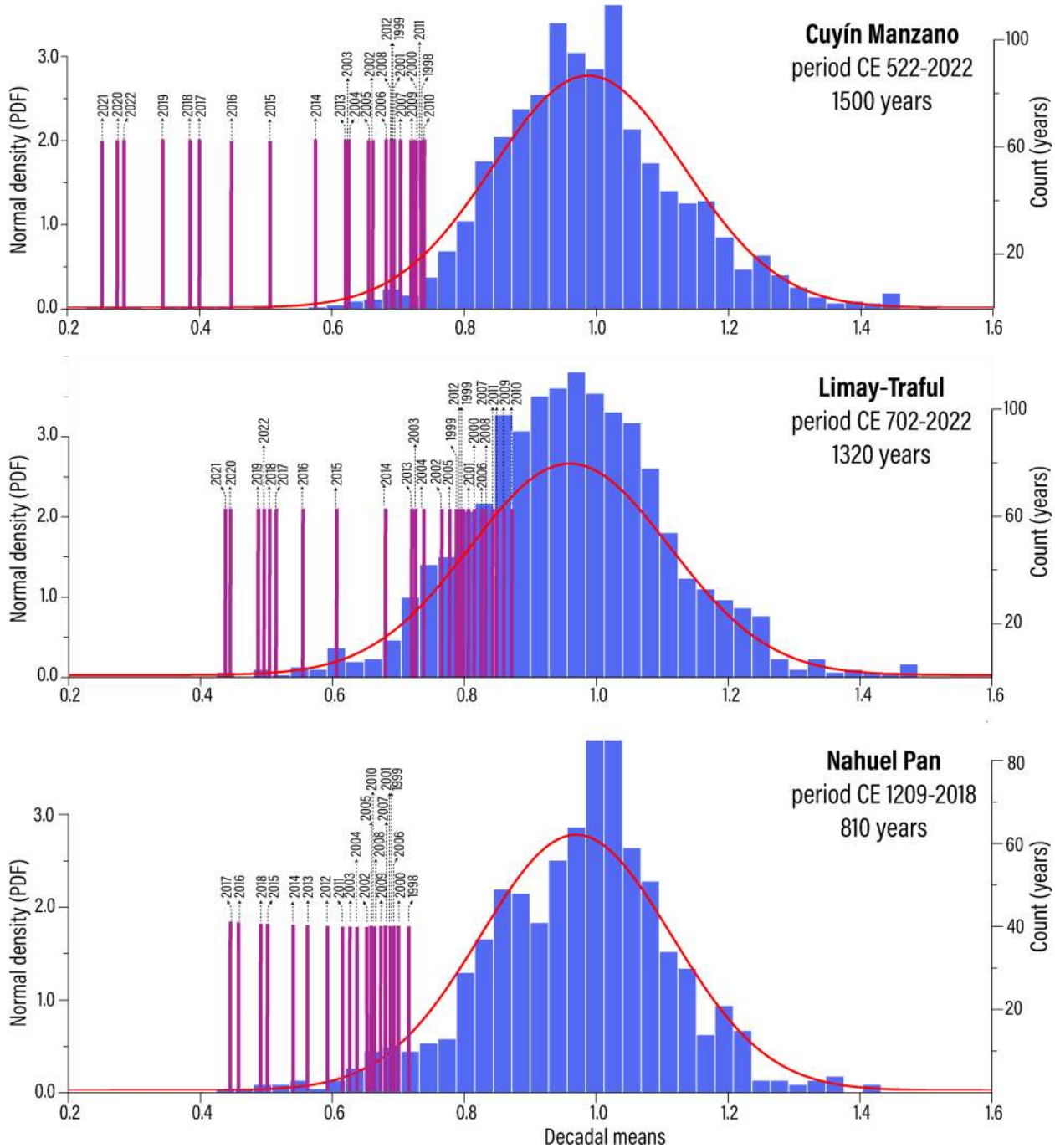


Fig. 7 Distributions of right-aligned 10-year mean tree-ring indices for the Cuyín Manzano, Confluencia Limay-Traful, and Cerro Nahuel Pan chronologies over the interval with EPS > 0.85 (Table 1). Blue histograms show the empirical distribution of all decadal means, where the value for year *t* represents the mean for years *t* − 9 to *t*. Red curves show the fitted normal distributions based on the sample mean and standard deviation of the respective decadal means. Vertical lines indicate the most recent decadal windows ending between 1998 and 2022

(Fig. 8). Across the full record, the maximum run length of consecutive decadal windows ≤ P5 is 27 decadal windows (1996–2022), underscoring the exceptional persistence of the modern downturn. The non-overlapping decade analysis supports the same inference: the most recent decade (2013–2022) is the lowest among all 150 non-overlapping decades, and the three most recent non-overlapping decades (1993–2002, 2003–2012,

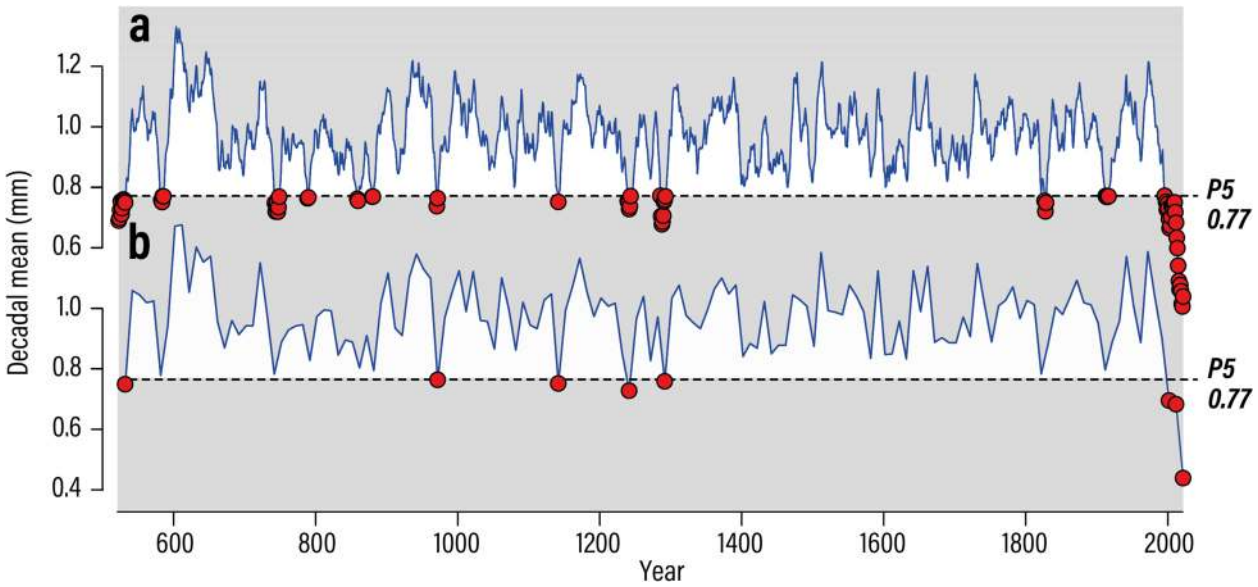


Fig. 8 Highly persistent and extreme recent low-growth regimes in the regional chronology. **a** In the overlapping decadal-window series, all 27 windows ending in 2022 lie at or below the 5th percentile threshold (P5; run length = 27), and the minimum value reaches 0.405 mm in the 2009–2018 window, placing the recent interval in the extreme lower tail of the historical distribution. Across the full record, the maximum run length of consecutive windows ≤ P5 is also 27 (1996–2022), highlighting the exceptional persistence of the modern downturn. **b** The non-overlapping decade analysis leads to the same qualitative conclusion: the most recent decade (2013–2022) is the lowest among all 150 non-overlapping decades, and the three most recent decades (1993–2002, 2003–2012, and 2013–2022) form a consecutive three-decade run below the non-overlapping P5 threshold (P5 = 0.769)

2013–2022) form a continuous three-decade run below the non-overlapping P5 threshold (P5 = 0.770; Fig. 8).

Circular block bootstrap simulations further show that this pattern is highly unlikely under a stationary, autocorrelated null model. The probability of reproducing a segment with 25 of 25 decadal windows ≤ P5 remains extremely low across block lengths ($p < 0.0005$ for $L = 10$; 0.0005 for $L = 20$; 0.001 for $L = 30$; 0.011 for $L = 50$). Likewise, the probability of obtaining a segment minimum as low as that observed is also very small ($p = 0.0010$, 0.0075, 0.0110, and 0.0165 for $L = 10$, 20, 30, and 50, respectively). Taken together, these independent diagnostics converge on the same conclusion: the 1998–2022 interval represents an exceptionally persistent and statistically extreme low-growth regime relative to the background variability of the last 1500 years.

Climate–growth relationships

Previous studies have consistently shown that radial growth of *Austrocedrus chilensis* is primarily controlled by hydroclimatic variability, particularly spring–summer temperature and moisture conditions in northern Patagonia (Villalba et al. 1998; Marcotti et al. 2025). To assess whether recent growth reductions remain consistent with this historical sensitivity, we evaluated the extent to which interannual growth variability can be accounted for by the main temperature and moisture controls identified during the instrumental period (Fig. 9).

All regression models were fitted over the common 1917–2022 period ($n = 106$). Among the individual predictors, October–March temperature emerged as the strongest climatic control on long-term regional growth of *A. chilensis*. Its negative effect explained a substantial and highly significant fraction of interannual growth variability (*Adj.* $r^2 = 0.359$; Table S2), clearly outperforming annual precipitation accumulated from the previous May to the current April, which showed a weaker, although still significant, positive relationship (*Adj.* $r^2 = 0.213$). This contrast was also reflected in model accuracy, with lower prediction errors for temperature (*RMSE* = 0.225) than for precipitation alone (*RMSE* = 0.249). Combining temperature and precipitation substantially improved model performance (*Adj.* $r^2 = 0.420$; *RMSE* = 0.213), indicating that both variables provide complementary information on interannual growth variability. Model skill increased further when a medium-term water-balance metric (SPEI-48) was added, yielding the best overall performance among all tested models (*Adj.* $r^2 = 0.458$; *RMSE* = 0.205; *MAE* = 0.163). Information criteria (*AIC*/*BIC*) consistently favored this three-predictor model, supporting the inclusion of accumulated hydroclimatic stress as an important additional constraint on regional growth variability (Table S2).

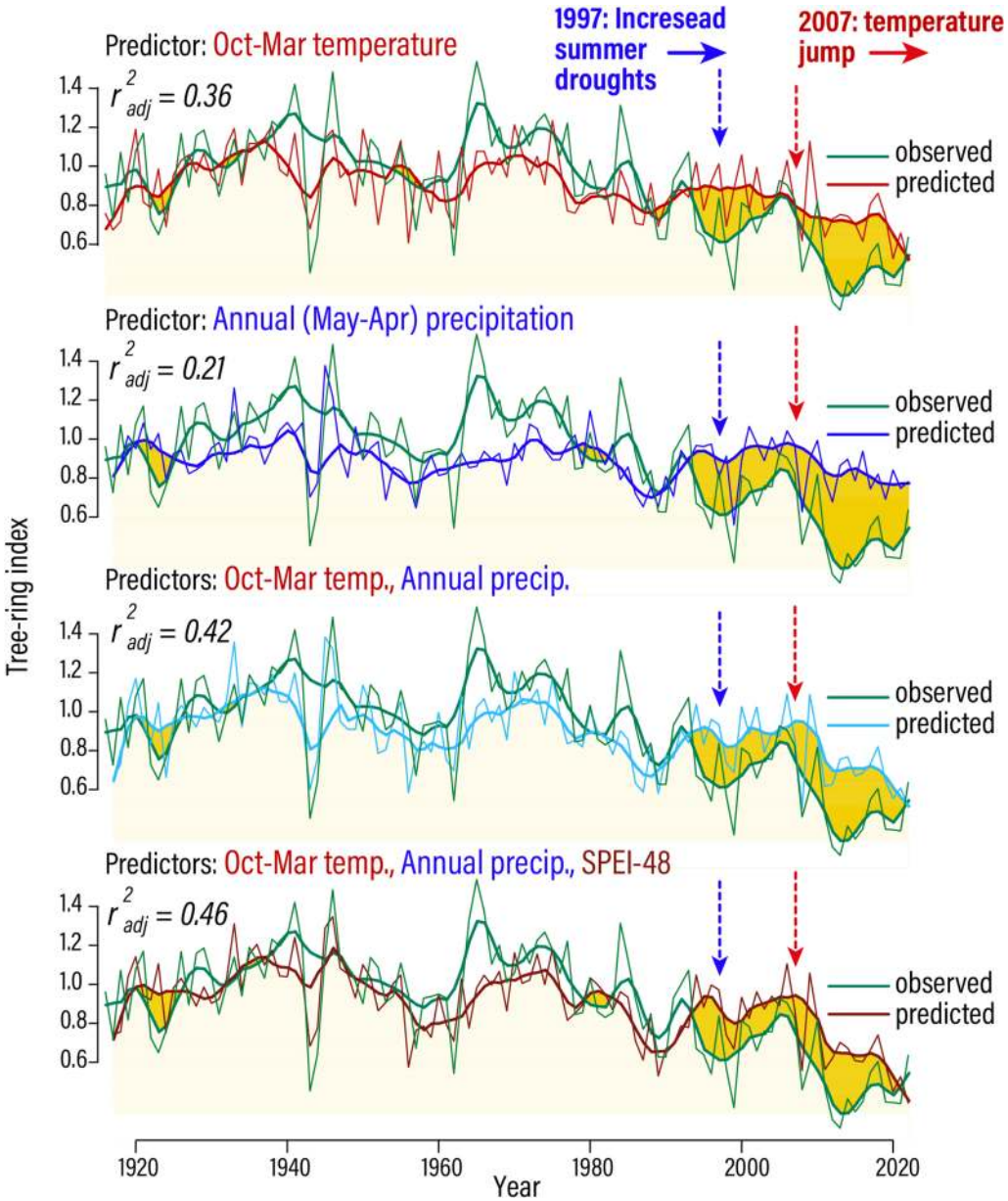


Fig. 9 Regional growth chronology of *A. chilensis* in the forest–steppe ecotone and its relationships with hydroclimatic variability over the last century. Observed and predicted regional growth variations are shown for regression models relating tree-ring indices to: **a** mean October–March temperature anomaly; **b** annual precipitation anomaly (May–April); **c** October–March temperature and annual precipitation; and **d** October–March temperature, annual precipitation, and SPEI-48 calculated for February of the growing season. Adjusted r^2 values are given for the full 1917–2020 period. The yellow-shaded interval highlights the climate–growth decoupling since the mid-1990s, during which observed growth remained consistently lower than predicted from hydroclimatic conditions

Despite the improved fit obtained by incorporating a predictor with multi-year memory, residual diagnostics still revealed significant positive autocorrelation in all models (Durbin-Watson < 2; Ljung-Box $p < 0.001$ up to lag 10). This indicates that an important component of temporal persistence in growth remains unexplained by these linear regressions, even when SPEI-48 is included. Together, these results point to strong temporal dependence in *A. chilensis* growth and suggest that memory or carry-over processes are intrinsic components of the climate–growth relationship.

Recent climate–growth expectations

Although model performance improved progressively with the inclusion of additional climatic predictors, this gain did not eliminate the divergence between observed and predicted growth in recent decades (Fig. S5). Across all models, comparisons between observed and predicted values reveal a sustained increase in residuals beginning in the mid-1990s, followed by a sharp intensification of the divergence after 2012. The increasingly negative residuals indicate that growth in recent decades was systematically lower than expected from hydroclimatic conditions alone. This pattern is evident in models calibrated over the full 1917–2022 period (Fig. S5) but becomes even clearer when models are calibrated only over 1917–1997, before the onset of the strong residual divergence (Fig. 10). Systematic negative residual departures become apparent from approximately 1994 onward. However, we selected 1997 as the end of the calibration period because it marks the beginning of a significant increase in the frequency of extreme summer droughts in the region (Fig. 3).

A reference climate model calibrated over 1917–1997 using standardized October–March temperature (zT) and May–April annual precipitation (zP) reproduced regional chronology variability reasonably well during the calibration interval ($r^2 \approx 0.31$), but its performance declined markedly when extrapolated to 1994–2022. The fitted coefficients had the expected signs, with growth increasing under wetter conditions (positive zP) and decreasing under warmer conditions (negative zT). When applied beyond the calibration period, however, residuals shifted abruptly toward negative values beginning in the mid-1990s (Fig. 10). Throughout 1994–2022, residuals remained predominantly below zero, indicating that the contemporaneous-climate model systematically overestimated observed growth; that is, growth was consistently lower than expected from temperature and precipitation alone (Fig. 10a). The mean residual during 1994–2022 was approximately − 0.31, compared with 0 by construction during calibration, and the bias became stronger toward the end of the record.

To evaluate whether this unexplained component of growth was related to antecedent hydroclimatic stress, we linked annual residuals from the temperature–precipitation model to SDI_prev5, an index of compounded stress over the previous five years. Residuals showed a significant negative association with SDI_prev5, such that years preceded by greater accumulated stress tended to exhibit more negative residuals and therefore lower growth than expected under current-year climate conditions (Fig. 10a, b). Using the P80 threshold of SDI_prev5 during 1917–1997, the high antecedent-stress regime showed significantly more negative mean residuals than the low-stress regime under HAC(1)-based inference, consistent with a regime shift associated with drought legacy effects (Fig. 10d).

A HAC(1)-robust regression of residuals on antecedent stress for 1994–2022 yielded a negative slope (≈ -0.074), consistent with the expectation that stronger prior stress leads to lower-than-expected growth. However, the effect was only marginal at conventional significance levels ($p(\text{HAC}) \approx 0.083$; $n = 29$), suggesting that the relationship may be nonlinear and/or threshold-dependent. Threshold analysis identified an optimal cutoff at $\tau \approx -0.185$ in SDI_prev5. Years with SDI_prev5 $\geq \tau$ ($n = 23$) showed a much more negative mean residual (− 0.344) than years with SDI_prev5 $< \tau$ ($n = 6$; mean residual = − 0.173; Fig. 12d). The regime difference (high minus low) was − 0.172 and remained strongly significant under HAC(1) inference ($p \approx 9.33 \times 10^{-5}$). This pattern indicates an abrupt increase in model overestimation once antecedent conditions cross a critical threshold, consistent with legacy-driven decoupling.

The quintile step-response analysis reinforced this interpretation. Mean residuals became progressively more negative with increasing SDI_prev5 from Q1 to Q4, with the strongest departure in Q4 (mean $\approx -0.465 \pm 0.032$ *SE*). This stepwise shift supports the hypothesis that repeated warm droughts progressively push trees outside the climate–growth relationship established during the reference period (1917–1997). The non-monotonic behavior in Q5 may reflect saturation effects, limited sample size, or a shift in limiting factors under the most extreme antecedent stress.

(See figure on next page.)

Fig. 10 Emergence of climate–growth decoupling and antecedent composite stress during 1994–2022. **a** Annual residuals calculated as observed minus predicted growth from a baseline climate–growth model (regional chronology ~ $zP + zT$) calibrated over 1917–1997. **b** Antecedent stress summarized by SDI_prev5, defined as the mean SDI over the previous five years (t–1 to t–5). **c** Relationship between residuals and SDI_prev5, with the dashed line indicating the threshold (τ) identified by grid search. **d** Mean residuals for the low- and high-stress regimes defined by τ. **e** Residual distributions for years with SDI_prev5 below and above τ. **f** Mean residuals across SDI_prev5 quintiles; error bars indicate ± 1 standard error. Increasingly negative residuals with higher antecedent stress indicate persistent growth suppression beyond that predicted by contemporaneous temperature and precipitation alone, consistent with drought legacy effects

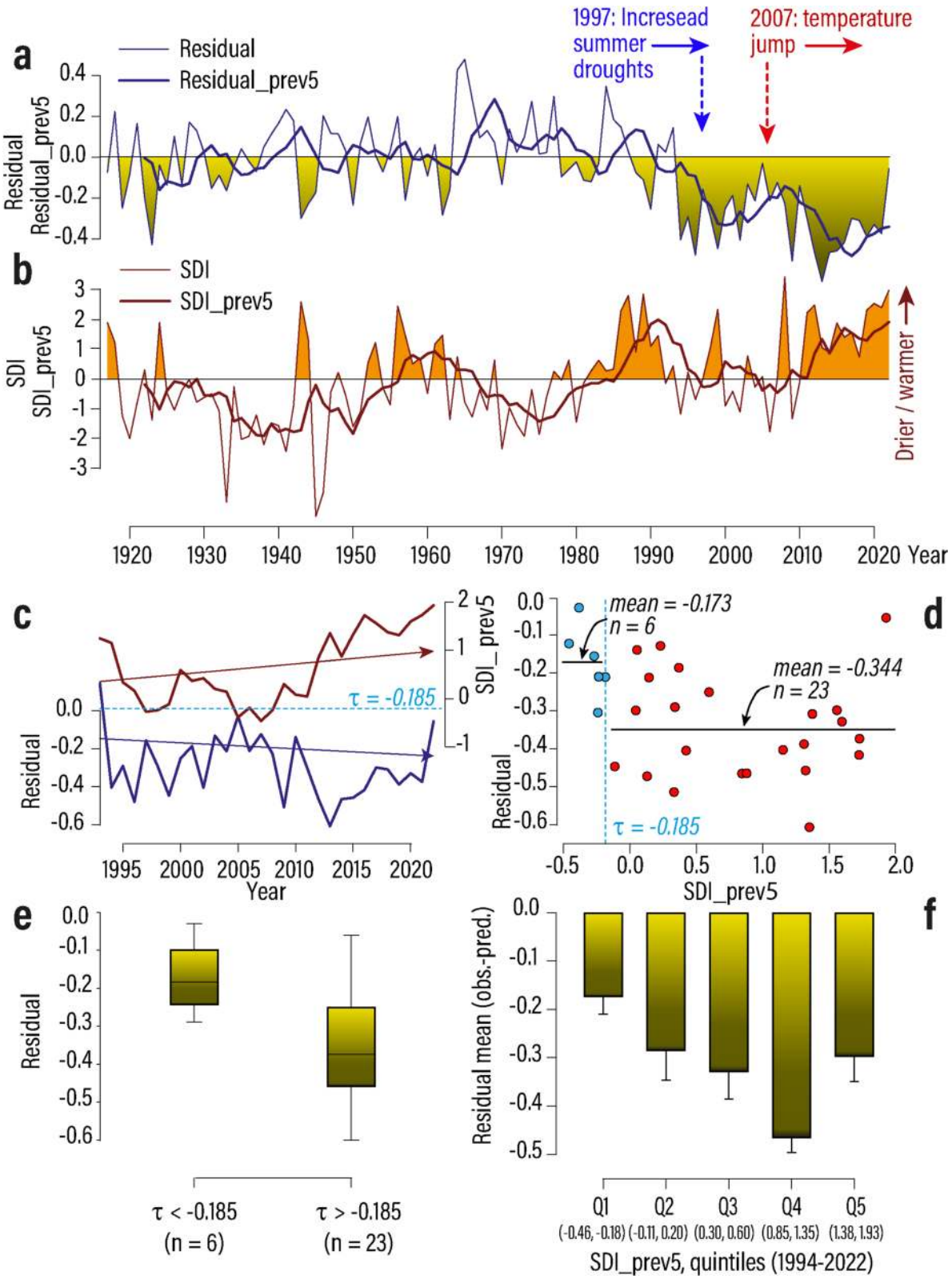


Fig. 10 (See legend on previous page.)

Drought legacy effects

The association between increasingly negative residuals and antecedent hydroclimatic stress suggests that recent climate–growth divergence may reflect not only a weakening of the contemporaneous climate signal, but also the emergence of persistent post-drought effects. To evaluate this possibility, we compared the temporal persistence of growth anomalies before and after 1994 using event-based analyses.

Event-based analyses further showed that drought impacts became more persistent in the modern period. In the SEA of regional growth (Fig. 11a), post-1994 drought events exhibited lower composite growth anomalies than pre-1994 events from the event year onward, with the strongest contrast during years $t = +4$ and $t = +5$. At $t = 0$, mean growth anomaly was − 1.28 for pre-1994 events and − 2.55 for post-1994 events; for $t = +4$ and $t = +5$, post-1994 anomalies remained strongly negative (− 2.48 and − 2.37), whereas pre-1994 values were much closer to zero (− 0.25 and − 0.03).

In the SEA of model residuals (Fig. 11b), pre-1994 events showed relatively modest negative anomalies at $t = 0$ (− 0.76) and $t = +1$ (− 0.68), followed by recovery toward near-zero or positive values from approximately $t = +2$ (0.33) and $t = +3$ (0.55). In contrast, post-1994 events maintained negative residual anomalies from $t = 0$ (− 2.09) through at least $t = +7$, indicating prolonged growth suppression beyond that predicted by climate alone; this contrast was especially marked during years $t = +4$ and $t = +5$, when post-1994 residual anomalies remained strongly negative (− 1.83 and − 2.52, respectively).

To quantify this difference, we computed an event-level persistence metric (Good 2005) as the mean residual anomaly over post-drought years ($t = +1$ to $+7$) and compared pre-1994 and post-1994 groups using a one-sided permutation test. The observed group difference was − 1.852 (post-1994 minus pre-1994), with a one-sided permutation $p = 0.0079$, indicating significantly stronger persistence of negative growth anomalies after 1994.

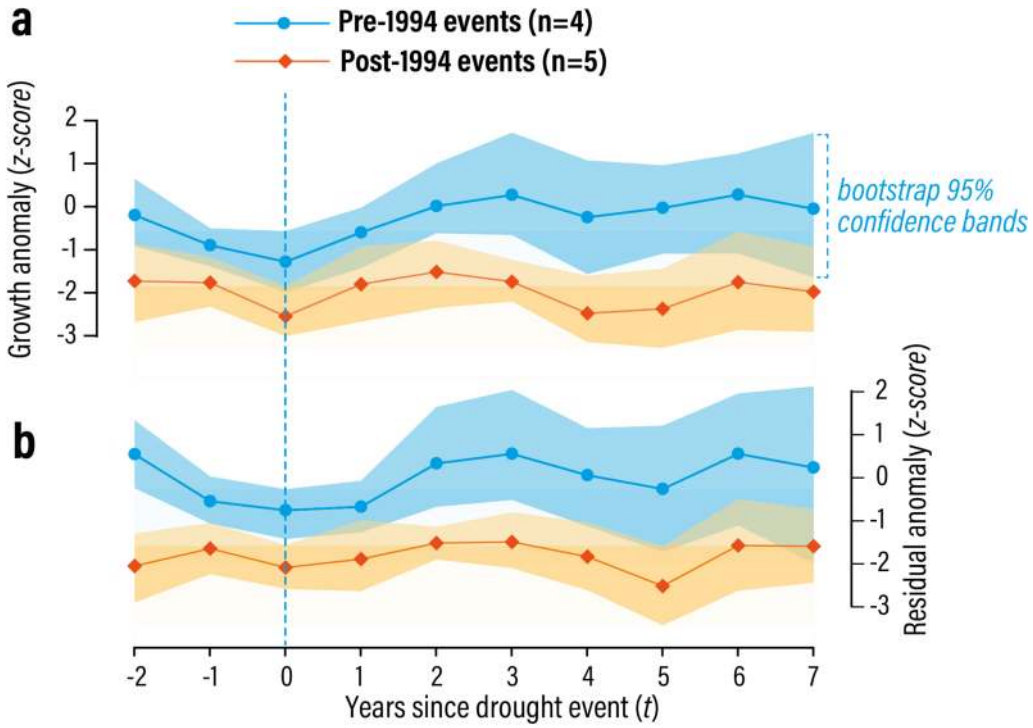


Fig. 11 Superposed epoch analysis (SEA) of drought-related growth persistence in the regional *A. chilensis* chronology. **a** SEA of regional tree growth aligned to drought-event years ($t = 0$; vertical dashed line), comparing pre-1994 events (1958, 1962, 1979, and 1989; $n = 4$) with post-1994 events (1999, 2004, 2008, 2015, and 2019; $n = 5$). **b** SEA of growth residuals (observed minus climate-predicted growth) aligned to drought-event years ($t = 0$), comparing the same pre-1994 and post-1994 event groups. Shaded bands indicate bootstrap 95% confidence intervals based on event resampling with replacement. Post-1994 events show lower growth trajectories and more persistent negative residual anomalies than pre-1994 events. The sustained post-drought reduction in growth (**a**), together with persistently negative residuals after $t = 0$ (**b**), indicates growth suppression that exceeds expectations from the historical climate–growth relationship, consistent with stronger drought legacy effects in the modern period

Discussion

An unprecedented recent decline in tree growth

The recent decline in *A. chilensis* growth at the Patagonian forest–steppe ecotone cannot be interpreted simply as another expression of interannual drought sensitivity within the range of past tree-growth variability. Instead, our results indicate the emergence of a persistent low-growth regime that is exceptional in the context of the last 1800 years. Independent evidence from nearby *A. chilensis* records provides additional regional context for this interpretation. A well-replicated ring-width chronology, including successfully cross-dated remnant wood, was recently developed northeast of El Bolsón (Amoroso et al. 2018). Situated between Cuyín Manzano and Cerro Nahuel Pan, the Condor Ridge chronology (41°56′S, 71°22′W) shows persistently below-average growth from 2008 to 2015, following a long-term decline from a period of maximum growth that ended in 1977. This recent episode of markedly suppressed growth appears to be unprecedented in the Condor Ridge record extending back to 1629 and is consistent with the extensive tree mortality observed across the site (Amoroso et al. 2018). In addition, a network of 28 *A. chilensis* chronologies from the northern Patagonian Andes shows a persistent reduction in growth from 1977 to the end of the record in 2014, with values consistently below the long-term mean. This sustained decline is unprecedented over at least the last 300 years (Marcotti et al. 2025). Although these comparisons do not constitute a formal spatial consistency test, the agreement between these independent records and the decline documented across our three study sites and in the regional chronology supports the interpretation that recent growth reductions in *A. chilensis* reflect a regional rather than purely local pattern.

Our results indicate that the semiarid ecotonal *A. chilensis* forests in northern Patagonia may be experiencing growth conditions outside the envelope of natural variability that characterized most of the late Holocene. This millennial perspective provides the foundation for interpreting the recent decline as a response to a changing hydroclimatic regime rather than as a short-lived fluctuation within the natural range of past variability.

Recent warming and intensified droughts

The hydroclimatic analyses further show that this recent shift toward lower growth occurred under a marked transition to warmer and drier conditions in northern Andean Patagonia (Garreaud 2018; Masiokas et al. 2019). Instrumental data show sustained warm-season warming, an increase in the frequency of extreme summer droughts, and persistent multi-year moisture deficits during recent decades. The warming trend identified in October–March temperatures at both Bariloche and Esquel is consistent with previous evidence of regional warming across the northern Patagonian Andes (Villalba et al. 2003; Masiokas et al. 2008; Rusticucci et al. 2016). In addition, the thermal breakpoints detected in both records may reflect broader reorganizations in Pacific and Southern Hemisphere climate variability, including the mid-1970s shift in atmospheric circulation described in previous studies (Mantua et al. 1997; Villalba et al. 2003; Vuille et al. 2018).

Our climate–growth analyses demonstrate the negative association between warm-season temperature and regional growth, and the positive association between precipitation and regional growth, confirming that both evaporative demand and moisture availability constrain growth variability (Fig. 9). The explanatory regression models of *A. chilensis* growth show that including long-memory hydroclimatic metrics such as SPEI48, in addition to temperature and precipitation, modestly improved the explained variance, especially by reducing regression residuals during the last decade (Fig. S5). This supports the idea that cumulative water deficits are ecologically relevant for *A. chilensis* at the ecotone. These results fit well with the view that drought stress in this environment is not only the consequence of a single dry growing season but can also build over multiple years through sustained moisture limitation.

The ecotonal setting of the studied *A. chilensis* populations is critical for interpreting our climate–growth relationships. Semiarid forest–steppe boundaries are typically characterized by strong moisture limitation, so even moderate warming can intensify growth constraints by increasing evaporative demand and reducing effective water availability (Kitzberger 2012). Under such conditions, persistent warm droughts are likely to exert disproportionate effects on radial growth, especially when they recur over short intervals. Our findings therefore demonstrate that the recent decline is closely linked to a regional intensification of hydroclimatic stress rather than to isolated drought years alone.

Climate–growth relationships under recent warm-dry conditions

The regression and residual analyses indicate that, although temperature and moisture availability explain a substantial fraction of historical growth variability, the increasing overestimation of observed growth after the mid-1990s points to a progressive weakening of the historical climate–growth relationship. The recent low-growth pattern therefore cannot be interpreted simply as the continuation of the same climate–growth relationship operating under more extreme climatic forcing. Instead, the data suggest that trees have tended to

perform worse under the modern warm-dry regime than would be expected from the twentieth-century model. In other words, climate still matters, but contemporaneous climate variables alone are no longer sufficient to account for the observed magnitude of growth reduction. This interpretation is supported by the increasingly negative residuals in recent decades, which indicate systematic underperformance relative to expectations derived from the historical model (Fig. 10).

At the same time, our results do not demonstrate a complete breakdown of climate control, nor do they by themselves establish a fully non-stationary climate–growth relationship (Peltier and Ogle 2020; Peltier et al. 2022). Rather, they indicate that recent growth suppression is only partly explained by the climatic predictors that described tree growth during the reference period. The inclusion of long-memory predictors such as SPEI48 improved model performance only modestly and did not eliminate the recent increase in residual values between predicted and observed growth (González de Andrés et al. 2025). This suggests that the modern reduction in growth cannot be fully captured by yearly climate alone, even when cumulative moisture deficits are considered. In that sense, the mismatch between observed and predicted growth is more consistent with the increasing influence of antecedent stress and post-drought carry-over effects than with a simple intensification of the historical climate–growth response (Peltier and Ogle 2020; Peltier et al. 2022).

Drought legacy effects

The association between increasingly negative residuals, higher antecedent hydroclimatic stress, and prolonged post-drought suppression suggests that recent growth decline is being shaped not only by current-year climate, but also by drought legacy effects. The event-based analyses, which exclude consecutive drought years as independent events, provide complementary evidence for this interpretation by showing more persistent post-drought suppression in the recent period. Post-1994 drought events were associated with lower growth trajectories and more persistent negative residual anomalies than pre-1994 events (Fig. 11). Residuals remained negative for several years after recent droughts, whereas earlier events showed more limited departures and faster recovery toward expected growth levels. Because residual anomalies represent variation not explained by the baseline climate model, their persistence after drought years is consistent with the interpretation of drought legacy effects (Gazol et al. 2017). Taken together, these results suggest that the post-1994 decoupling reflects not only lower-than-expected growth under recent hydroclimatic conditions, but also stronger post-drought persistence. Because residual departures are greatest under high antecedent stress and remain negative for several years after drought events, the recent low-growth regime appears to reflect a combination of intensified warm-dry conditions, reduced predictability from the historical climate–growth relationship, and enhanced drought legacy effects.

These legacy effects likely reflect carry-over processes that reduce growth capacity beyond the event year, such as incomplete hydraulic recovery, depletion of carbon reserves, canopy damage, or sustained reductions in cambial activity (Anderegg et al. 2015). Our data do not allow direct identification of the underlying physiological mechanism, so this interpretation should remain cautious. Nevertheless, the combination of threshold-like residual behaviour, stronger post-drought persistence in recent decades, and declining agreement with the historical model, suggests that growth resilience has weakened under recent repeated warm-drought conditions. In this sense, the recent growth decline appears to reflect not only a more severe effect of climatic forcing, but also a reduced capacity of ecotonal forests to recover growth rates between successive drought events. This interpretation is especially relevant to explain the persistence of recent low-growth conditions.

If repeated droughts leave lasting effects on hydraulic function, carbon balance, crown condition, or cambial activity, then each new event may act on trees that have not fully recovered from previous stress. Under this scenario, radial growth may become increasingly shaped by ecological memory and reduced recovery capacity (Anderegg et al. 2015; Marcotti et al. 2021; Peltier et al. 2022). The recent growth decline in *A. chilensis* may therefore be understood not simply as a direct response to recent negative hydroclimatic changes, but as the cumulative outcome of repeated warm-dry conditions and incomplete post-drought recovery.

The broader implication of these findings is that *A. chilensis* forests at the semiarid forest–steppe ecotone in northern Patagonia may be entering a phase of heightened vulnerability under continued warming and recurrent drought. Moreover, our results reinforce the importance of incorporating antecedent stress and drought legacy processes into interpretations of forest responses to climate change. Tree growth at dry range margins may no longer respond solely to contemporaneous conditions, but increasingly to the cumulative effects of repeated moisture deficits and incomplete recovery.

Limitations and uncertainties

Detecting long-term growth trends in tree-ring chronologies remains methodologically challenging because standardization choices can influence the preservation

or removal of low-frequency variability. In this study, the recent decline in *A. chilensis* growth was consistently expressed across independent sites and alternative detrending approaches, supporting the robustness of the general pattern. However, the exact magnitude and long-term ranking of the decline should be interpreted with caution, because no single detrending method can fully separate age-related biological trends, disturbance-related growth variation, and environmentally driven low-frequency variability.

Additional uncertainties arise from changes in sample composition and replication through time, particularly in the earlier portions of long chronologies and near the end of the records, where recent changes are central to our interpretation. Although comparisons with nearby *A. chilensis* records support a regional-scale interpretation, these comparisons do not constitute a formal spatial consistency test. Similarly, our climate–growth and residual analyses indicate an increasing mismatch between observed growth and expectations from the historical climate–growth relationship, but they do not by themselves identify the physiological mechanisms underlying this pattern. Processes such as incomplete hydraulic recovery, carbon depletion, canopy damage, or reduced cambial activity remain plausible but untested mechanisms.

Therefore, our results should be interpreted as evidence for a persistent and regionally coherent reduction in radial growth under recent warm-dry conditions, rather than as a precise quantification of the absolute magnitude of the decline or a definitive attribution to a single causal mechanism. Despite these limitations, the consistency of the recent growth reduction across sites, detrending approaches, independent regional records, and climate–growth residual analyses supports the conclusion that the recent decline is not solely an artifact of chronology standardization.

Our findings also underscore the importance of long-term monitoring in *A. chilensis* forests at the forest–steppe ecotone. Identifying the most climatically sensitive stands and microsites may help inform conservation and adaptive management under ongoing warming and drought stress.

Conclusions

This study demonstrates that the recent decline in *Austrocedrus chilensis* growth at the forest–steppe ecotone in northern Patagonia is an exceptional event in terms of its magnitude and persistence when assessed in a long-term, millennial context. By placing recent radial-growth reductions in the context of the last 1500 years, the study shows that the current low-growth pattern lies outside the range of natural variability that characterized most of the late Holocene. The decline coincides with intensified warm-season warming, more frequent extreme droughts, and persistent multi-year moisture deficits. Although methodological uncertainties remain, the recent reduction in growth is consistently expressed across sites and detrending approaches. Increasingly negative residuals, their association with antecedent stress, and their prolonged persistence after recent drought events point to an increasing mismatch between observed growth and expectations from historical climate–growth responses. These findings indicate that recent ecotonal forest responses in northern Patagonia reflect not only intensified hydroclimatic stress but also declining growth resilience under present warm-drought conditions. Under continued warming and recurrent droughts, as projected for the northern Patagonian Andes during the current century (Pabón-Caicedo et al. 2020; Marianetti et al. 2026), the forest–steppe ecotonal *A. chilensis* populations may remain in a reduced-growth state and be subjected to negative demographic effects as long as the current hydroclimatic configuration persists.

Supplementary Information

The online version contains supplementary material available at https://doi.org/10.1186/s13717-026-00704-6.

Additional file 1.

Acknowledgements
We thank Marcelo Bourguet, Melisa Giménez, Andrés Lo Vecchio, and Adan Hajduk for their support during field sampling. We are also grateful to Daniela Mendoza for her assistance with tree-ring measurements. We further acknowledge members of the Laboratorio de Dendrocronología e Historia Ambiental, IANIGLA, CONICET, Mendoza, Argentina and the Laboratorio de Dendrocronología y Cambio Global, Universidad Austral de Chile, for their collaboration during field sampling campaigns.

Author contributions
DW and RV conceived the study and designed the sampling strategy, including the identification of strategic study sites, with contributions from CL and DC. All authors participated in different field sampling campaigns. DW processed samples, performed dendrochronological and statistical analyses, and wrote the original draft of the manuscript. RV provided overall scientific supervision, contributed to data interpretation, and participated in structuring the manuscript. EM and LMV processed samples from several of the study sites. TG assisted with tree-ring measurements. All authors read and approved the final manuscript.

Funding
This study was supported by CONICET—PIP N°0789CO; Volcanic-Induced severe droughts (VODSAM) LEFE-CNRS, AAP INSU 2025; Red Bosque-Clima, Programa de Redes Federales de Alto Impacto, Contribution number 37; Fundación Williams, Fondos Complementarios 2024, FONDECYT 1241699, 1262510; ANID/BASALFB210018. The funding bodies had no role in the design of the study, data collection, analysis, interpretation of the data, or in writing the manuscript.

Availability of data and material
The datasets generated and analyzed during the current study are available from the corresponding author upon reasonable request.

Declarations

Ethics approval and consent to participate
Not applicable.

Consent for publication
Not applicable.

Competing interests
The authors declare no competing interests.

Author details
[1]Instituto Argentino de Nivología, Glaciología y Ciencias Ambientales (IANIGLA-CONICET), Universidad Nacional de Cuyo (UNCuyo), Gobierno de Mendoza, Av. Dr. Ruiz Leal s/n, Parque General San Martín, M5500 Mendoza, Argentina. [2]Laboratorio de Dendrocronología y Cambio Global, Instituto de Conservación Biodiversidad y Territorio, Universidad Austral de Chile, Campus Isla Teja s/n, Valdivia, Chile. [3]Center for Climate and Resilience Research (CR)2, Blanco Encalada 2002, 4th Floor, FCFM, Universidad de Chile, Santiago, Chile. [4]Cape Horn International Center (CHIC), O'Higgins 310, 6350000 Puerto Williams, Cabo de Hornos, Chile. [5]Instituto de Datación y Arqueometría (InDyA), CONICET, Provincia de Jujuy, UNT, UNJu, CNEA AR, Av. Martijena s/n, Palpalá, 4612 Jujuy, Argentina. [6]Naturalis Biodiversity Center, Darwinweg 2, 2333 CR Leiden, The Netherlands. [7]Facultad de Ciencias Exactas y Naturales, Universidad Nacional de Cuyo, Padre Jorge Contreras 1300, M5502JMA Mendoza, Argentina.

Received: 13 March 2026 Accepted: 13 May 2026
Published: 8 June 2026

References

Amoroso MM, Daniels LD, Larson BC (2012) Temporal patterns of radial growth in declining *Austrocedrus chilensis* forests in northern Patagonia: the use of tree rings as an indicator of forest decline. For Ecol Manag 265:62–70. https://doi.org/10.1016/j.foreco.2011.10.021

Amoroso M, Speer JH, Daniels LD, Villalba R, Cook E, Stahle DW, Srur A, Tardif J, Conciatori F, Aciar E, Arco J, Bonada A, Coulthard B, Haney J, Isaac-Renton M, Magalhães J, Marcotti E, Meglioli P, Montepeluso MS, Oelkers R, Pearl J, Pompa-García M, Robson J, Rodríguez Catón M, Soto P, Young A (2018) South American Dendroecological Fieldweek 2016: exploring dendrochronological research in northern Patagonia. Tree Ring Res 74(1):120–131. https://doi.org/10.3959/1536-1098-74.1.120

Anderegg WRL, Schwalm C, Biondi F, Camarero JJ, Koch G, Litvak M, Ogle K, Shaw JD, Shevliakova E, Williams AP, Wolf A, Ziaco E, Pacala S (2015) Pervasive drought legacies in forest ecosystems and their implications for carbon cycle models. Science 349(6247):528–532. https://doi.org/10.1126/science.aab1833

Bai J, Perron P (1998) Estimating and testing linear models with multiple structural changes. Econometrica 66(1):47–78

Bai J, Perron P (2003) Computation and analysis of multiple structural change models. J Appl Econom 18(1):1–22

Boisier JP, Alvarez-Garreton C, Cordero RR, Damiani A, Gallardo L, Garreaud RD, Lambert F, Ramallo C, Rojas M, Rondanelli R (2018) Anthropogenic drying in central-southern Chile evidenced by long-term observations and climate model simulations. Elementa 6:74. https://doi.org/10.1525/elementa.328

Boninsegna JA, Argollo J, Aravena JC, Barichivich J, Christie D, Ferrero ME, Lara A, Le Quesne C, Luckman BH, Masiokas M, Morales M, Oliveira JM, Roig F, Srur A, Villalba R (2009) Dendroclimatological reconstructions in South America: a review. Palaeogeogr Palaeoclimatol Palaeoecol 281(3–4):210–228. https://doi.org/10.1016/j.palaeo.2009.07.020

Briffa KR (1990) Basic chronology statistics and assessment. In: Kairiukstis LA, Cook ER (eds) Methods of dendrochronology: Applications in the environmental sciences. Kluwer Academic Publishers, pp 137–152

Briffa KR, Melvin TM (2011) A closer look at regional curve standardization of tree-ring records: Justification of the need, a warning of some pitfalls, and suggested improvements in its application. In: Hughes MK, Swetnam TW, Diaz HF (eds) Dendroclimatology: Progress and prospects. Springer, pp 113–145

Cook ER, Kairiukstis LA (1990) Methods of dendrochronology: applications in the environmental sciences. Kluwer Academic Publishers

Cook ER, Krusic PJ (2005) ARSTAN: A tree-ring standardization program based on detrending and autoregressive time series modeling, version 49. Columbia University, Lamont-Doherty Earth Observatory

Cook ER, Briffa KR, Meko DM, Graybill DA, Funkhouser G (1995) The segment length curse in long tree-ring chronology development for paleoclimatic studies. Holocene 5:229–237

Deng K, Azorin-Molina C, Yang S, Hu C, Zhang G, Minola L, Chen D (2022) Changes of Southern Hemisphere westerlies in the future warming climate. Atmos Res 270:106040. https://doi.org/10.1016/j.atmosres.2022.106040

Donoso Zegers C (1993) Bosques templados de Chile y Argentina. Variación, estructura y dinámica. Editorial Universitaria

Dussaillant I, Berthier E, Brun F, Masiokas M, Hugonnet R, Favier V, Rabatel A, Pitte P, Ruiz L (2019) Two decades of glacier mass loss along the Andes. Nat Geosci 12(10):802–808. https://doi.org/10.1038/s41561-019-0432-5

Efron B, Tibshirani RJ (1993) An introduction to the bootstrap. Chapman & Hall/CRC

Fritts HC (1976) Tree rings and climate. Academic Press

Garreaud R (2018) Record-breaking climate anomalies lead to severe drought and environmental disruption in western Patagonia in 2016. Clim Res 74(3):217–229. https://doi.org/10.3354/cr01505

Garreaud RD, Vuille M, Compagnucci R, Marengo J (2009) Present-day South American climate. Palaeogeogr Palaeoclimatol Palaeoecol 281(3–4):180–195

Garreaud R, Lopez P, Minvielle M, Rojas M (2013) Large-scale control on the Patagonian climate. J Clim 26(1):215–230. https://doi.org/10.1175/JCLI-D-12-00001.1

Garreaud RD, Alvarez-Garreton C, Barichivich J, Boisier JP, Christie D, Galleguillos M, Le Quesne C, McPhee J, Zambrano-Bigiarini M (2017) The 2010–2015 megadrought in central Chile: impacts on regional hydroclimate and vegetation. Hydrol Earth Syst Sci 21(12):6307–6327. https://doi.org/10.5194/hess-21-6307-2017

Gazol A, Camarero JJ, Anderegg WRL, Vicente-Serrano SM (2017) Impacts of droughts on the growth resilience of Northern Hemisphere forests. Glob Ecol Biogeogr 26:166–176. https://doi.org/10.1111/geb.12526

González de Andrés E, Fajardo A, Camarero JJ, Fernández-Cortés Á, Gazol A (2025) Surviving a megadrought: shifts in climate sensitivity of an austral conifer in Chile due to persistent water shortage. Agric For Meteorol 373:110791. https://doi.org/10.1016/j.agrformet.2025.110791

González-Reyes Á, Christie DA, Schneider-Valenzuela I, Venegas-González A, Muñoz AA, Hadad M, Gipoulou-Zuñiga T, Tapia-Marzan V, Gibson-Carpintero S, Santini-Junior L, Le Quesne C, Villalba R (2024) Recent multispecies tree-growth decline reveals a severe aridity change in Mediterranean Chile. Environ Res Lett 19(6):064046. https://doi.org/10.1088/1748-9326/ad4049

Good PI (2005) Permutation, parametric, and bootstrap tests of hypotheses, 3rd edn. Springer

Goyal R, Sen Gupta A, Jucker M, England MH (2021) Historical and projected changes in the Southern Hemisphere surface westerlies. Geophys Res Lett 48(4):e2020GL090849. https://doi.org/10.1029/2020GL090849

Gyenge JE, Fernandez ME, Dalla Salda G, Schlichter T (2005) Leaf and whole-plant water relations of the Patagonian conifer *Austrocedrus chilensis* (D. Don) Pic. Ser. et Bizzarri: implications for its drought resistance capacity. Ann For Sci 62(4):297–302. https://doi.org/10.1051/forest:2005024

Hadad MA, González-Reyes Á, Roig FA, Matskovsky V, Cherubini P (2021) Tree-ring-based hydroclimatic reconstruction for the northwest Argentine Patagonia since 1055 CE and its teleconnection to large-scale atmospheric circulation. Glob Planet Change 202:103496. https://doi.org/10.1016/j.gloplacha.2021.103496

Holmes RL (1983) Computer-assisted quality control in tree-ring dating and measurement. Tree-Ring Bull 43:69–77

Hurtado SI, Calianno MHJ, Adduca S, Easdale MH (2023) Drylands becoming drier: evidence from North Patagonia, Argentina. Reg Environ Change 23:1–13. https://doi.org/10.1007/s10113-023-02035-2

Kannenberg SA, Novick KA, Alexander MR, Maxwell JT, Moore DJP, Phillips RP, Anderegg WRL (2019) Linking drought legacy effects across scales: from

leaves to tree rings to ecosystems. Glob Change Biol 25(9):2978–2992. https://doi.org/10.1111/gcb.14710
Kitzberger T (2012) Ecotones as complex arenas of disturbance, climate, and human impacts: the trans-Andean forest-steppe ecotone of Northern Patagonia. In: Myster RW (ed) Ecotones Between Forest and Grassland. Springer, pp 59–88. https://doi.org/10.1007/978-1-4614-3797-0_3
Kitzberger T, Veblen TT, Villalba R (1997) Climatic influences on fire regimes along a rain forest-to-xeric woodland gradient in northern Patagonia, Argentina. J Biogeogr 24:35–47
Künsch HR (1989) The jackknife and the bootstrap for general stationary observations. Ann Stat 17(3):1217–1241
Lahiri SN (2003) Resampling methods for dependent data. Springer. https://doi.org/10.1007/978-1-4757-3803-2
LaMarche VC Jr, Holmes RL, Dunwiddie PW, Drew LG (1979) Tree-ring chronologies of the Southern Hemisphere: 1. Laboratory of Tree-Ring Research, University of Arizona, Argentina (Chronology Series V)
Larsson L-Å (2010) CDendro & CooRecorder: Image-based tree-ring analysis. Cybis Elektronik & Data AB
Le Quesne C, Stahle DW, Cleaveland MK, Therrell MD, Aravena JC, Barichivich J (2006) Ancient *Austrocedrus* tree-ring chronologies used to reconstruct central Chile precipitation variability from AD 1200 to 2000. J Clim 19(22):5731–5744
Lloyd-Hughes B, Saunders MA (2002) A drought climatology for Europe. Int J Climatol 22:1571–1592
Mantua NJ, Hare SR, Zhang Y, Wallace JM, Francis RC (1997) A Pacific interdecadal climate oscillation with impacts on salmon production. Bull Am Meteorol Soc 78(6):1069–1079
Marcotti E, Amoroso MM, Rodríguez-Catón M, Vega L, Srur AM, Villalba R (2021) Growth resilience of *Austrocedrus chilensis* to drought along a precipitation gradient in Patagonia, Argentina. For Ecol Manage 496:119388. https://doi.org/10.1016/j.foreco.2021.119388
Marcotti E, Villalba R, Rodríguez-Catón MR, Srur AM, Boninsegna JA, Amoroso MM (2025) Climate-growth relationships and paleoclimate potential of *Austrocedrus chilensis* revisited by extending its tree-ring network in Argentina. Dendrochronologia 90:126309. https://doi.org/10.1016/j.dendro.2025.126309
Marianetti G, Rivera JA, Bettolli ML (2026) A dry and warm future projected by regional climate models in the subtropical Andes Mountains, southwestern South America. Earth Syst Environ. https://doi.org/10.1007/s41748-026-01032-7
Masiokas MH, Villalba R, Luckman BH, Lascano ME, Delgado S, Stepanek P (2008) 20th-century glacier recession and regional hydroclimatic changes in northwestern Patagonia. Glob Planet Change 60(1–2):85–100. https://doi.org/10.1016/j.gloplacha.2006.07.031
Masiokas MH, Cara L, Villalba R, Pitte P, Luckman BH, Toum E, Christie DA, Le Quesne C, Mauget S (2019) Streamflow variations across the Andes (18°–55°S) during the instrumental era. Sci Rep 9(1):17879. https://doi.org/10.1038/s41598-019-53981-x
Maxwell RS, Larsson L-Å (2021) Measuring tree-ring widths using the CooRecorder software application. Dendrochronologia 67:125841. https://doi.org/10.1016/j.dendro.2021.125841
McKee TB, Doesken NJ, Kleist J (1993) The relationship of drought frequency and duration to time scales. In: Proceedings of the 8th Conference on Applied Climatology, Anaheim, 17–22 January 1993, pp 179–184
Melvin TM, Briffa KR (2008) A "signal-free" approach to dendroclimatic standardisation. Dendrochronologia 26(2):71–86. https://doi.org/10.1016/j.dendro.2007.12.001
Miranda A, Syphard AD, Berdugo M, Carrasco J, Gómez-González S, Ovalle JF, Delpiano CA, Vargas S, Squeo FA, Miranda MD, Dobbs C, Mentler R, Lara A, Garreaud R (2023) Widespread synchronous decline of Mediterranean-type forest driven by accelerated aridity. Nat Plants 9(11):1810–1817. https://doi.org/10.1038/s41477-023-01541-7
Morales MS, Cook ER, Barichivich J, Christie DA, Villalba R, LeQuesne C, Srur AM, Ferrero ME, González-Reyes Á, Couvreux F, Matskovsky V, Aravena JC, Lara A, Mundo IA, Rojas F, Prieto MR, Smerdon JE, Bianchi LO, Masiokas MH, Urrutia-Jalabert R, Rodriguez-Catón M, Muñoz AA, Rojas-Badilla M, Alvarez C, Lopez L, Luckman BH, Lister D, Harris I, Jones PD, Williams AP, Velazquez G, Aliste D, Aguilera-Betti I, Marcotti E, Flores F, Muñoz T, Cuq E, Boninsegna JA (2020) Six hundred years of South American tree rings reveal an increase in severe hydroclimatic events since mid-20th century. Proc Natl Acad Sci USA 117(29):16816–16823. https://doi.org/10.1073/pnas.2002411117
Mudelsee M (2010) Climate time series analysis: classical statistical and bootstrap methods. Springer. https://doi.org/10.1007/978-3-319-04450-7
Mundo IA, El Mujtar VA, Perdomo MH, Gallo LA, Villalba R, Barrera MD (2010) *Austrocedrus chilensis* growth decline in relation to drought events in northern Patagonia, Argentina. Trees 24(3):561–570. https://doi.org/10.1007/s00468-010-0427-8
Newey WK, West KD (1987) A simple, positive semi-definite, heteroskedasticity and autocorrelation consistent covariance matrix. Econometrica 55(3):703–708. https://doi.org/10.2307/1913610
O'Connor GK, Steig EJ, Hakim GJ (2021) Strengthening Southern Hemisphere westerlies and Amundsen Sea Low deepening over the 20th century revealed by proxy-data assimilation. Geophys Res Lett 48:e2021GL095999. https://doi.org/10.1029/2021GL095999
Pabón-Caicedo JD, Espinoza JC, Andina A, Arias PA, Bettolli ML, Garreaud R, Insarov G, Lavado-Casimiro W, Ramírez-Villegas J, Samaniego N, Viale M (2020) Observed and projected hydroclimate changes in the Andes. Front Earth Sci 8:61. https://doi.org/10.3389/feart.2020.00061
Pastorino M, Aparicio A, Azpilicueta MM (2015) Regiones de procedencia del ciprés de la cordillera y bases conceptuales para el manejo de sus recursos genéticos en Argentina. Ediciones INTA
Peltier DMP, Ogle K (2020) Tree growth sensitivity to climate is temporally variable. Ecol Lett 23(11):1561–1572. https://doi.org/10.1111/ele.13575
Peltier DMP, Anderegg WRL, Guo JS, Ogle K (2022) Contemporary tree growth shows altered climate memory. Ecol Lett 25(12):2663–2674. https://doi.org/10.1111/ele.14130
Pettitt AN (1979) A non-parametric approach to the change-point problem. Appl Stat 28:126–135
Politis DN, Romano JP (1992) A circular block-resampling procedure for stationary data. In: LePage R, Billard L (eds) Exploring the limits of bootstrap. Wiley, New York, pp 263–270
Rao MP, Cook ER, Cook BI, Anchukaitis KJ, D'Arrigo RD, Krusic PJ, LeGrande AN (2019) A double bootstrap approach to superposed epoch analysis to evaluate response uncertainty. Dendrochronologia 55:119–124. https://doi.org/10.1016/j.dendro.2019.05.001
Reig-Gracia F, Latorre Garcés B (2023) SPEIbase v2.9. DIGITAL.CSIC. https://doi.org/10.20350/digitalCSIC/15470
Reiter EJ, Weigel R, Walentowski H, Loguercio GA, Fierke J, Neri Winter AF, Simon A, Kotowska MM, Joelson NZ, Caselli M, Leuschner C (2024) Climate vulnerability of *Nothofagus pumilio*, *Nothofagus dombeyi* and *Austrocedrus chilensis* in northern Patagonia's temperate forests. For Ecol Manag 572:122261. https://doi.org/10.1016/j.foreco.2024.122261
Rivera JA, Penalba OC, Villalba R, Araneo DC (2017) Spatio-temporal patterns of the 2010–2015 extreme hydrological drought across the Central Andes, Argentina. Water 9(9):652. https://doi.org/10.3390/w9090652
Rivera JA, Otta S, Lauro C, Zazulie N (2021) A decade of hydrological drought in Central-Western Argentina. Front Water 3:640544. https://doi.org/10.3389/frwa.2021.640544
Rodríguez-Catón M, Villalba R, Morales M, Srur A (2016) Influence of droughts on *Nothofagus pumilio* forest decline across northern Patagonia, Argentina. Ecosphere 7(7):e01390. https://doi.org/10.1002/ecs2.1390
Rusticucci M, Kyselý J, Almeira G, Lhotka O (2016) Long-term variability of heat waves in Argentina and recurrence probability of the severe 2013–2014 summer heat wave. J Clim 29(10):3651–3669. https://doi.org/10.1175/JCLI-D-15-0614.1
Schulman E (1956) Dendroclimatic changes in semiarid America. University of Arizona Press
Schwarz G (1978) Estimating the dimension of a model. Ann Stat 6(2):461–464
Stokes M, Smiley T (1968) An introduction to tree-ring dating. University of Chicago Press
Veblen TT, Burns BR, Kitzberger T, Lara A, Villalba R (1995) The ecology of the conifers of southern South America. In: Enright NJ, Hill RS (eds) Ecology of the Southern Conifers. Melbourne University Press, Melbourne
Veblen TT, Kitzberger T, Villalba R, Donnegan J (1999) Fire history in northern Patagonia: the roles of humans and climatic variation. Ecol Monogr 69(1):47–67
Veblen TT, Donoso C, Kitzberger T, Rebertus A (1996) Ecological processes in southern South American forests. In: Veblen TT, Hill RS, Read J (eds) The ecology and biogeography of Nothofagus forests. Yale University Press, New Haven, pp 293–353

Vega LM, Marcotti E, Amoroso MM (2019) Variación en los patrones de crecimiento previo a la muerte de individuos de *Austrocedrus chilensis* a lo largo de un gradiente pluviométrico en el norte de la Patagonia Andina. Ecol Austral 29(2):297–310. https://doi.org/10.25260/EA.19.29.2.0.778
Vega LM, Daux V, Srur AM, Villalba R (2025) Physiological response of *Austrocedrus chilensis* (Cupressaceae) to climatic drought: a stable isotope and growth perspective. Trees 39(6):114. https://doi.org/10.1007/s00468-025-02693-z
Viale M, Bianchi E, Cara L, Ruiz LE, Villalba R, Pitte P, Masiokas M, Rivera J, Zalazar L (2019) Contrasting climates at both sides of the Andes in Argentina and Chile. Front Environ Sci 7:69. https://doi.org/10.3389/fenvs.2019.00069
Vicente-Serrano SM, Beguería S, López-Moreno JI (2010) A multiscalar drought index sensitive to global warming: the SPEI. J Clim 23(7):1696–1718. https://doi.org/10.1175/2009JCLI2909.1
Villalba R, Veblen TT (1997a) Spatial and temporal variation in *Austrocedrus* growth along the forest-steppe ecotone in northern Patagonia. Can J For Res 27(4):580–597. https://doi.org/10.1139/x96-209
Villalba R, Veblen TT (1997b) Regional patterns of tree population age structures in northern Patagonia: climatic and disturbance influences. J Ecol 85:113–124
Villalba R, Veblen TT (1998) Influences of large-scale climatic variability on episodic tree mortality in northern Patagonia. Ecology 79:2624–2640. https://doi.org/10.2307/176506
Villalba R, Cook E, Jacoby GC, D'Arrigo RD, Veblen TT, Jones PD (1998) Tree-ring based reconstructions of northern Patagonia precipitation since AD 1600. Holocene 8(6):659–674. https://doi.org/10.1191/095968398669095576
Villalba R, Lara A, Boninsegna JA, Masiokas M, Delgado S, Aravena JC, Roig FA, Schmelter A, Wolodarsky A, Ripalta A (2003) Large-scale temperature changes across the Southern Andes: 20th-century variations in the context of the past 400 years. In: Diaz HF (ed) Climate variability and change in high elevation regions: past, present & future, vol 15. Springer, Netherlands, pp 177–232. https://doi.org/10.1007/978-94-015-1252-7_10
Villalba R, Lara A, Masiokas M, Urrutia R, Luckman BH, Marshall GJ, Mundo IA, Christie DA, Cook ER, Neukom R, Allen K, Fenwick P, Boninsegna JA, Srur AM, Morales M, Araneo D, Palmer J, Cuq E, Le Quesne C (2012) Unusual southern hemisphere tree growth patterns induced by changes in the Southern Annular Mode. Nat Geosci 5(11):793–798. https://doi.org/10.1038/ngeo1613
Villamayor J, Khodri M, Villalba R, Daux V (2021) Causes of the long-term variability of Southwestern South America precipitation in the IPSL-CM6A-LR model. Clim Dyn 57(9):2391–2414. https://doi.org/10.1007/s00382-021-05811-y
von Storch H, Zwiers FW (1999) Statistical analysis in climate research. Cambridge University Press
Vuille M, Carey M, Huggel C, Buytaert W, Rabatel A, Jacobsen D, Soruco A, Villacis M, Yarleque C, Timm OE, Condom T, Salzmann N, Sicart J-E (2018) Rapid decline of snow and ice in the tropical Andes: impacts, uncertainties and challenges ahead. Earth Sci Rev 176:195–213. https://doi.org/10.1016/j.earscirev.2017.09.019
Wang S, Hu M, Chen F, Zhao X, Hadad MA, Roig FA, Meko DM, Torbenson MCA, Piraino S, Zhang H, Xu Y, Chen Y, Yue W, Cao H (2025) Recent South-central Andes water crisis driven by Antarctic amplification is unprecedented over the last eight centuries. Commun Earth Environ 6(1):937. https://doi.org/10.1038/s43247-025-02858-1
Wigley TML, Briffa KR, Jones PD (1984) On the average value of correlated time series, with applications in dendroclimatology and hydrometeorology. J Clim Appl Meteorol 23(2):201–213. https://doi.org/10.1175/1520-0450(1984)023%3c0201:OTAVOC%3e2.0.CO;2
Wilks DS (2011) Statistical methods in the atmospheric sciences, 3rd edn. Academic Press
Zeileis A, Leisch F, Hornik K, Kleiber C (2002) Strucchange: an R package for testing for structural change in linear regression models. J Stat Softw 7(2):1–38. https://doi.org/10.18637/jss.v007.i02

Publisher's Note

Springer Nature remains neutral with regard to jurisdictional claims in published maps and institutional affiliations.